energies

MDPI

Article

Improvement of Extracted Power of Pole Mounted Solar Panels by Effective Cooling Using Aluminum Heat Sink under Hot Weather and Variable Wind Speed Conditions

Youssef Hassan [1,2], Mohamed Orabi [1], Abdulaziz Alshreef [2], Omar M. Al-Rabghi [3], Badr A. Habeebullah [3], Abdelali El Aroudi [4,*] and Mohamed A. Ismeil [1,5]

1 Aswan Power Electronics Applications Research Center (APEARC), Faculty of Engineering, Aswan University, Aswan 81542, Egypt; yousef.badry@aswu.edu.eg (Y.H.); orabi@ieee.org (M.O.); melzanaty@apearc.aswu.edu.eg (M.A.I.)

2 Department of Electrical and Computer Engeneering, King Abdulaziz University, P.O. Box 80204, Jeddah 21589, Saudi Arabia; alshareef1379@yahoo.com

3 Department of Mechanical Engeneering, King Abdulaziz University, P.O. Box 80204, Jeddah 21589, Saudi Arabia; orabghi@kau.edu.sa (O.M.A.-R.); bhabeeb@kau.edu.sa (B.A.H.)

4 Departament d'Enginyeria Electrònica, Universitat Rovira i Virgili, Elèctrica i Automàtica, 43007 Tarragona, Spain

5 Faculty of Engineering, South Valley University, Qena 83523, Egypt

* Correspondence: abdelali.elaroudi@urv.cat

Received: 12 May 2020; Accepted: 12 June 2020; Published: 18 June 2020

Abstract: The increase in operating temperature of PV generators leads to degradation of their performance. These adverse effects of high temperatures are considered as one of the most important problems that solar panel operation faces in hot weather areas. A lot of research has been undertaken to study this aspect and find ways of limiting the harm caused by such high temperatures. To overcome this harm and to maintain the operating temperature of the PV cells within the optimum range specified by manufacturers, cooling the solar panels often becomes indispensable. This paper discusses the heat transfer through the solar panel layers and studies the effect of high temperature on the solar panel performance in a hot desert environment. It also presents the development of a new solar panel structure viz. by installing an aluminum heat sink to reduce the effect of temperature rise and thus improve the solar panel performance. The study focuses on a pole-mounted solar panel for a street lighting apparatus in extremely hot desert conditions with fluctuating wind speeds. It will be shown that adding an aluminum heat sink to the solar panel bottom mitigates the effect of increased temperature and hence modifies the solar panel operating point by increasing both the efficiency and the lifetime. The solar cell temperature is decreased by 16.4% as a result of the aluminum heat sink installation on the solar panel back sheet and consequently, the accumulated energy produced by the the solar panel is increased by 13.23% per day.

Keywords: solar panel performance; photovoltaic (PV) cell; heat sink; back surface cooling of photovoltaic panel; solar panel and excessive heat

1. Introduction

Saudi Arabia is a leader in the field of fossil oil production in the Middle Eastern Gulf region. Nevertheless, in the recent years the country has made strides in harnessing new renewable energy sources to meet its energy requirements, mostly owing to the environmental sustainability of these energy sources [1]. Several investigations about solar radiation have been carried in Jeddah City

(Saudi Arabia) which is considered a good example of a severe temperature case with the highest solar radiation values [2]. This research focuses on temperature mitigation of solar cells using a new improvement in solar panel structure. A literature review of the previous studies was performed. Many studies have indicated a reduction of the efficiency of solar panels under high temperature conditions [3–5]. Most traditional solutions are concerned with mitigation of the temperature effect via front surface cooling [6–12]. In [6] the active cooling is done by using power from 12 V 5.4 W batteries. The harvested energy has been compared to that obtained from the same source at a reference temperature of 20 °C, and a reduction of 45.5% was observed. In [7] active cooling has been used to study the effect of cooling on the PV characteristics, and it has been found that the module surface temperature has a direct effect on the open circuit voltage. The cooling increases the potential difference from 59 V to 62.3 V. In [8], a 2.6% increase in efficiency has been recorded with a 4.7% decrease in temperature. In addition, an increase of up to 8.4% has been recorded in the maximum power achieved. Uniform cooling has been presented in [9,10] where the temperature has been found to decrease non-uniformly from an average of 3 °C to 1.8 °C by employing jet cooling. Back surface cooling using water has been presented in [11–13]. This system achieved an increase in output power by about 12.5%. A new direction for solar panel cooling depends on the design of thermal and optical characteristics of a solar cell by limiting the parasitic absorption by selective spectral cooling, and then by improving the radiative cooling [14]. All previous cooling systems are classified as active cooling systems which use electrical devices and mechanical systems requiring extra power. On the other hand, passive cooling is deployed to decrease the temperature with the help of additional parts such as heat sinks [15–20] without requiring additional power input. In [15] by using a designed heat sink, the temperature reduction in the range of 30 °C–40 °C has been achieved. In [16], using both active and passive methods, heat is released out the heat sink by forced air. Although this system helps in reducing the temperature, the use of more than one method leads to an increase in the cost and this set-up suffers from the disadvantage of the large size of the needed exchanger as compared to the size of the PV cell. In [17] an aluminum heat sink has been used to dissipate the temperature of photovoltaic (PV) cells. Though, it has a lower coefficient of thermal conduction, the advantage is that it is cheaper. Increases of 20%, 13%, and 9% are achieved as regards efficiency, energy, and power conversion, respectively, by using the passive cooling technique. On the other hand, the energy can be increased by 14.4% at an ambient temperature of 15 °C. In [18] a simulation study has been done where the ribs of the heat sink have been demonstrated to decrease the temperate up to 10 °C below the normal temperature. In [19] heat sink fins increase the solar panel performance by increasing the cooling. The highest reduction obtained in solar panel temperature has been a decrease from 60.6 °C to 54.9 °C on average by employing a heat sink as a passive cooling methodology. This represents a 9.4% reduction in the temperature, and it causes an increase in the average output power by of about 15.3%. However, this study did not consider the variations of wind speed. Also, no design and selection for the heat sink has been performed. In [20] the cooling has been done by a heat sink as well as forced air and an average reduction of 10 °C in temperature has been achieved. The decrease in temperature achieved by the heat sink results in an increase in the open circuit voltage Voc and maximum power Pmpp by 10% and 18.67%, respectively. In [21] a steady state analysis of solar radiation falling on the solar panel surface was performed to obtain the amount of useful energy as well as thermal energy losses. The present work studies the effect of attaching an aluminum heat sink to the solar panel back surface to enable the heat transfer by conduction from its base to the heat sink base plate and fins and then to the surrounding air. The mathematical model used here is based on the one that was derived in [21]. However, the studied structure is modified to include the wind speed variation that could be due to movement of vehicles on the road when this model is applied for pole mounted solar panel of a street lighting system. Design and selection of heat sink are also addressed in order to reduce the operating temperature of the solar cell. Therefore, the original study in [21] is extended here to provide the gained energy due to the proposed system of pole mounted solar panels by effective cooling using aluminum heat sink under hot weather and variable wind speed environment.

2. An Overview on Solar Panels

A solar panel is a device by which light energy is converted into electrical energy. A brief description of solar panel structure and its principles are presented below.

2.1. Solar Panel Structure

Figure 1 shows the structure of solar panel considered in this study. It contains solar cells that consist of a p-n junction-based silicon layer encapsulated within a very thin film of protective sheets. These sheets are attached to both back and front sides, and are fabricated with ethyl vinyl acetate (EVA). Polyethylene terephthalate (PET) was used to fabricate the back sheet because if its high strength. This results in protection of the solar cells in addition to the junction box where the electrical output power connection terminals are located [22,23].

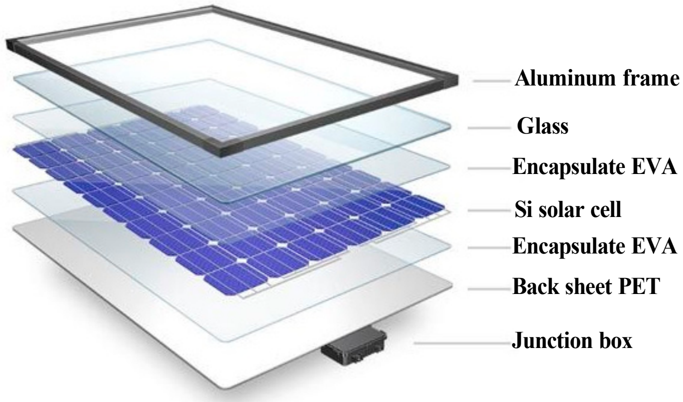

Figure 1. The material structure layers of a solar panel [22].

2.2. Solar Cell Principle of Operation

A solar cell is a p-n junction which is fabricated from silicon with few impurities. When the solar radiation strikes its surface, it forces the electrons to acquire enough energy so that electrons become free and an abundance of electron-hole pairs is created and a potential difference appears at the terminals. Then, an electric current flows if the circuit is connected to a load [24,25] as shown in Figure 2.

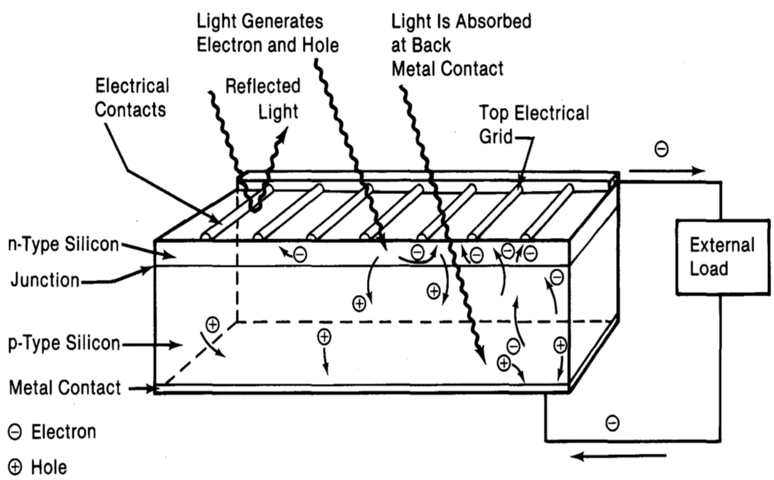

Figure 2. Principle of operation of a solar cell [24].

3. Solar Cell Energy Transmitted Mathematical Model

As sunlight falls on the surface of any solar cell, an amount of energy Q_C is trasmitted through the glass surface [21,26–30] given by the following Equation (1):

$$Q_C = f_p \alpha_C \tau_g S_r A \tag{1}$$

Figure 3 shows a cross-section of the solar panel as well as its thermal resistance network. The solar energy irradiating the solar panel Q_C is divided into two parts [21,31]; the useful energy and the thermal losses. The first part, i.e., the useful extracted energy, generates electrical energy Q_{el} according to the following expression:

$$Q_{el} = \eta_{el} Q_C \tag{2}$$

where η_{el} is the electrical efficiency given by:

$$\eta_{el} = \eta_o [1 - \beta (T_C - T_o)] \tag{3}$$

β is the temperature coefficient that relies on the material type (β = 0.004 K^{-1} for a monocrystalline solar cell fabricated from silicon [12,21]) and is given by Equation (4):

$$\beta = \frac{1}{T_C^* - T_o} \tag{4}$$

The nominal electrical efficiency η_o under the Standard Test Conditions (*STC*) is given by the Equation (5):

$$\eta_o = \frac{P_{mpp}}{Q_C} \tag{5}$$

As mentioned in [17,21], the P_{mpp} is the output power (W), that is tracked at the maximum power point (MPP), and given by Equation (6):

$$P_{mpp} = V_{mpp} I_{mpp} = V_{OC} I_{SC} FF \tag{6}$$

The second part is transformed into thermal energy losses Q_{th} that can be expressed as follows:

$$Q_{th} = \eta_{th} Q_C \tag{7}$$

where η_{th} is the thermal efficiency, given by:

$$\eta_{th} = \frac{U_L (T_C - T_a)}{f_p \alpha_C \tau_g S_r} \tag{8}$$

where U_L is the overall heat transfer coefficient, given by Equation (9):

$$U_L = U_t + U_b + U_e \tag{9}$$

where U_t, U_b and U_e are the heat transfer coefficients of top, bottom and edges, respectively, given in Equations (10)–(12):

$$U_t = \left(\frac{1}{R_{cd1} + R_{cd2} + (R_{cv1} || R_{r1})} \right) \tag{10}$$

$$U_b = \left(\frac{1}{R_{cd3} + R_{cd4} + (R_{cv2} || R_{r2})} \right) \tag{11}$$

$$U_e = \frac{A_e (k_e / t_e)}{A} \tag{12}$$

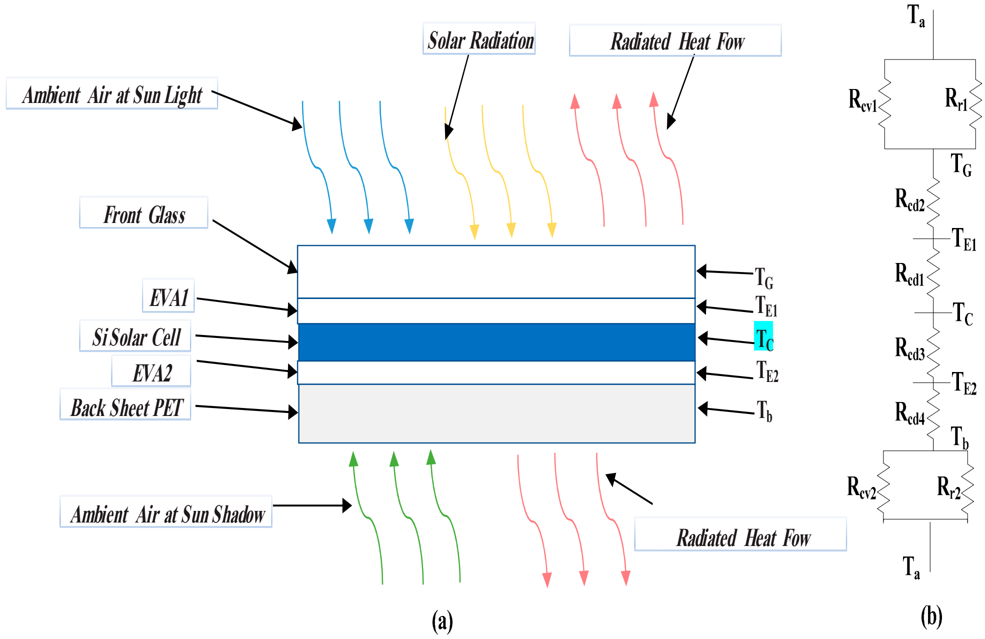

Figure 3. Solar panel (**a**) Cross-section (**b**) Thermal resistance network [21].

Table 1. Properties of the solar panel layers [21,23].

Layer Material	t (mm)	k (W/(m.K))	T	α	ε
Glass	4	0.78	0.90	0.02	0.91
Ethyl vinyl acetate (EVA)	0.4	0.34	0.97	0.03	0.85
Monocrystalline silicon	0.4	158.726	-	1	0.67
Polyethylene terephthalate (PET)	0.5	0.15	-	1	0.85
Silicon grease	0.5	2.2	-	-	-
Aluminum	0.5	239	-	-	0.90

The properties of the layers are listed in Table 1, where the reflection coefficient of the glass ζ= 0.1, indicating the solar radiation reflected from the surface of the glass [23]. The thermal resistance of any layer is given by Equation (13) for conduction and by Equation (14) for convection or radiation [21,32–34]:

$$R_{cd} = \frac{t}{kA} \tag{13}$$

$$R_{cv,or,r} = \frac{1}{h_{cv,or,r}A} \tag{14}$$

The heat transfer coefficient of back or front surfaces due to radiation effect $h_{r,f-a,or,b-a}$and the surrounding air heat transfer coefficient due to convection effect $h_{c,G-a,or,b-a}$are given by Equations (15)–(17):

$$h_{r,G-a,or,b-a} = \frac{\sigma\varepsilon_{G,or,b}\left(T_{G,or,b} + T_s\right)\left(T^2_{G,or,b} + T^2_s\right)\left(T_{G,or,b} - T_s\right)}{\left(T_{G,or,b} - T_a\right)} \tag{15}$$

$$h_{cv,G-a,or,b-a} = h_w = 5.74\omega_r^{0.8} L_{ch}^{-0.2} \tag{16}$$

$$h_{cv,G-a,or,b-a} = Nu\frac{k_a}{L_{ch}} \tag{17}$$

where L_{ch} is the surface characteristic length [35] as given in Equation (18), T_s is the sky temperature that is calculated by the empirical Equation (19), h_w is the convective heat transfer coefficient due to wind speed as defined in [36], (ω_r = 4–15 m/s) is the resultant wind speed due to the natural air wind speed (ω_s = 4 m/s) and the turbulence air (ω_t = 0–11 m/s) that is induced by movement of vehicles on the road as per Equations (20) and (21) as described in [21,37–40]:

$$L_{ch} = \frac{4A}{p} \tag{18}$$

$$T_s = 0.0552T_a^{1.5} \tag{19}$$

$$\omega_r = \omega_s + \omega_t \tag{20}$$

$$\omega_t = \sqrt{\left(\frac{n_v C_D A_{fv} \omega_v^3}{2c_e L_v}\right)^{\frac{2}{3}}} \tag{21}$$

As per Equations (20) and (21), the turbulence due to vehicles motion on the road accelerates the wind speed, which contributes to solar panel temperature reduction. As mentioned in [31,35], *Nu* is a Nusselt number that is calculated by Equation (22):

$$Nu = 0.664Re^{\frac{1}{2}}Pr^{\frac{1}{2}} \tag{22}$$

where *Re* is the Reynold number that is calculated using Equation (23) and *Pr* is the Prandtl number that is calculated using Equation (24):

$$Re = \frac{\rho \omega_r L_{ch}}{\mu} \tag{23}$$

$$Pr = \frac{\mu}{\lambda} \tag{24}$$

As shown in Figure 4, the heat transfer losses will be distributed in the top, bottom and edges directions [21,31,41] according to Equations (25)–(27) respectively:

$$Q_t = U_t A(T_C - T_a) \tag{25}$$

$$Q_b = U_b A(T_C - T_a) \tag{26}$$

$$Q_e = U_e A_e(T_C - T_a) \tag{27}$$

As mentioned in [29,41,42], the solar cell operating temperature (°C) is given by Equation (28):

$$T_C = T_a + \frac{NOCT - 20}{800} S_r \tag{28}$$

where *NOCT* indicates the normal operating cell temperature as per the manufacturer's datasheet. Tthe solar cell temperature T_C relies on the value of the solar radiation and the measured wind speed [43] as given by the empirical Equation (29):

$$T_C = T_a + (S_r.A)e^{-3.473-0.0594\omega_r} \tag{29}$$

To incorporate the effect of the wind speed on the convective heat transfer coefficient, a correlation shall be done in the cell temperature [31,43–46] for both Equations (28) and (29). Then, the solar cell temperature T_C is given, respectively, in the following approximate and accurate expressions:

$$T_C = T_a + \frac{S_r}{S_{r,NOCT}}(T_{NOCT} - T_{a,NOCT})\frac{9.5}{h_w}\left(1 - \frac{\eta_{el}}{\tau\alpha}\right) \tag{30}$$

$$T_C = T_a + \frac{S_r}{S_{r,NOCT}}(T_{NOCT} - T_{a,NOCT})\frac{U_{L,NOCT}}{U_L}\left(1 - \frac{\eta_{el}}{\tau\alpha}\right) \tag{31}$$

where $\tau\alpha$ = 0.9, $T_{a,NOCT}$ = 20 °C or 293 K, $S_{r,NOCT}$ = 800 W/m^2, $U_{L,NOCT}$ is the overall heat transfer coefficient at *NOCT*, wind speed is 1 m/s at *NOCT*. The analysis of the absorbed solar energy by the solar panel shall follow the energy balance [21,31], as per Equation (32), where the sum of the electrical and thermal efficiencies is equal to unity:

$$Q_C = Q_{el} + Q_{th} \tag{32}$$

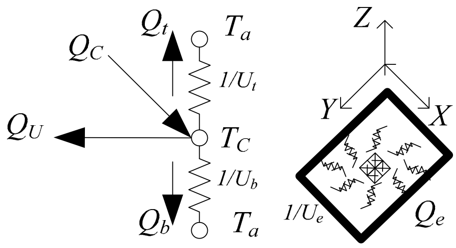

Figure 4. Equivalent thermal network of the solar panel (top, bottom and edge) [21].

4. Solar Energy Electrical Model

A single diode model of the solar cell is considered as the common electrical model, shown in Figure 5 for a solar panel that consists of n_c solar cells. The mathematical model of a single diode solar cell is shown in Appendix A. The output power P_{mpp} at the MPP is as given in Equation (6). Both the voltage and current at the MPP are calculated as mentioned in Appendix A by simultaneously and numerically solving Equations (A11) and (A12) or Equations (A13) and (A14) as in [21,24,30,31,47–50].

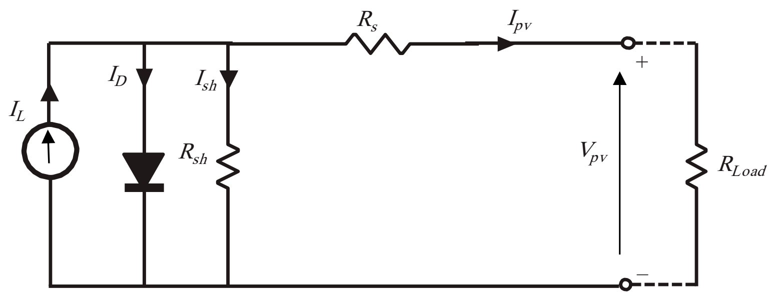

Figure 5. A single diode solar cell equivalent model [21].

5. The Methodology of Temperature Mitigation

The solar panel structure in this work is modified by installating an aluminum heat sink on its back sheet. First its shape will be selected and then its design will be performed. Finally, to obtain the experimental results, it will be assembled onto the solar panel back sheet.

5.1. Design and Selection of Aluminum Heat Sink

For this study, the heat sink is manufactured using aluminum and its shape is rectangular with length L (m), width W (m). It is connected by casting with N number of fins as shown in Figure 6a. The heat transfer from the source that has a temperature T_b to the heat sink surface via interface like a thermal grease used to fill any partial space between the heat source and sink to improve the thermal conductivity. The thermal network for heat exchange includes conduction, convection and radiation with ambient air as shown in Figure 6b [51,52]. The lumped heat sink thermal resistance R_{Hs} is presented by Equation (33):

$$R_{Hs} = R_{inr} + R_c + R_{sp} + R_{fins} + R_{fa} \tag{33}$$

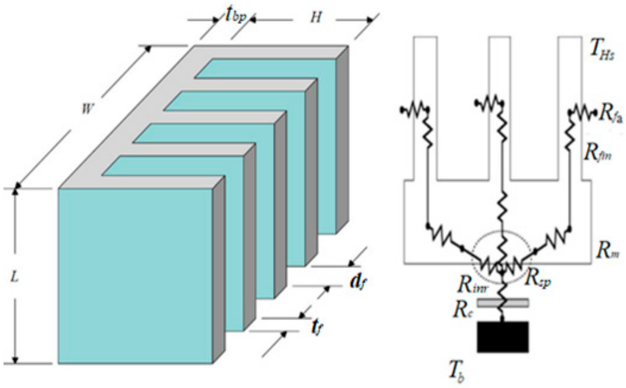

Figure 6. (**a**) Heat sink geometry, (**b**) Heat sink thermal resistance network [49].

The interface thermal resistance R_{inr} is given by Equation (13). It depends on the interface material conductivity k_r (W/m. K) and the surface area A (m^2) and it is inversely proportional to its thickness t_r (mm) [52]. Also, the contact resistance R_c between the heat source and the interface is given by Equation (13). It depends on the material properties and assembly method [51,53–56]. The spreading resistance is determined by the Equation (34):

$$R_{sp} = \frac{\psi_{av}}{\sqrt{\pi}kA} = \frac{1 - 1.410\varepsilon_r + 0.344\varepsilon_r^3 + 0.043\varepsilon_r^5 + 0.034\varepsilon_r^7}{4k\sqrt{A}} \quad (34)$$

where ψ_{av} is the dimensionless spreading resistance that is calculated as described in [54]. The adiabatic thermal resistance per each fin is given by Equation (35):

$$R_{fin} = \frac{1}{\tanh(mH)\sqrt{h_T p_f k A_f}} \quad (35)$$

where m is the fin parameter that is defined as a heat transfer ratio between the heat transfer of a finite length fin and an infinite length fin at identical medium conditions and it is given by Equation (36). To minimize the error due to the dimensional fins when considering the thermal energy analysis [32], it is necessary to achieve ($h_T.t_f/k < 0.2$):

$$m = \sqrt{\frac{h_T p}{kA_f}} \quad (36)$$

The lumped thermal resistance of total number of fins (N_f) can be calculated as a parallel circuit by Equation (37):

$$R_{fins} = \frac{1}{N_f/R_{fin} + (N_f - 1)R_{bpb}} \quad (37)$$

where R_{bpb} is the thermal resistance of the back heat sink base plate, given by Equation (13). The thermal resistance R_{fa} from the heat sink fins to ambient air is calculated by Equation (14) as a parallel convection and radiation thermal resistances. The total heat transfer rate Q_{fT} from the heat sink fins surface is calculated by Equation (38):

$$Q_{fT} = Q_{fins} + Q_{unfins} = h_T(\eta_{fins}A_{fins} + A_{unfins})(T_{Hs} - T_a) \quad (38)$$

For rectangular shape fins, the efficiency η_{fins} is given by Equation (39):

$$\eta_{fins} = \frac{\tanh(mH)}{mH} \quad (39)$$

As mentioned in [51,56], the optimum spacing d_f between the fins is given by Equation (40):

$$d_f = 2.714 \frac{H}{\sqrt[4]{R_a}} \tag{40}$$

where Ra is Rayleigh number that is equal to the multiplication of Prandtl number Pr and Grashoff number Gr as in Equation (41):

$$Ra = Pr.Gr = \frac{g\delta\Delta T_m L_{ch}^3}{\mu\lambda} \tag{41}$$

where T_m is the mean absorbed cell temperature as given in Equation (42), ΔT is the temperature difference between solar panel layers (K) as in Equation (43):

$$T_m = \frac{T_C + T_{G,or,b}}{2} \tag{42}$$

$$\Delta T = T_C - T_{G,or,b} \tag{43}$$

The optimum total number of fins N_f is given by Equation (44):

$$N_f = \frac{W - t_f}{d_f + t_f} + 1 \tag{44}$$

The aluminum heat sink selection depends on Equations (13), (14) and (33)–(44), using the data of Table 1 and the solar module dimensions as listed in Table 2. Properties of the thermal grease that was used as an interface between the solar panel and the aluminum heat sink has been specified in Table 3. A computational MATLAB software program was used to calculate the required heat sink parameters that matched Figure 6a, the obtained results as recorded in Table 4, where the aluminum thermal conductivity is equal to 239 W/m.K [57,58].

Table 2. Characteristics of the solar panel [21]. Standard Test Conditions (STC): Irradiance 1000 W/m^2, Module Temperature 25 °C, Air Mass 1.5.

Parameters of Solar Module	Values & Units
Brand/Cell type	BLT/Monocrystalline
Maximum Power	250 W
Power tolerance range	±3%
Module efficiency	23.6%
Voltage at open circuit $V_{o.c}$	36.7 V
Current at short circuit $I_{s.c}$	9 A
Maximum power voltage V_{mp}	30.6 V
Maximum power current I_{mp}	8.17 A
Normal operating cell temperature ($NOCT$)	45 ± 2 °C
Temperature Coefficient of $V_{o.c}$	−0.32%/°C
Geometric (Length × Width × Hight)	1646 × 990 × 45 mm
n_C (number of solar cells in series)	60
α_C	0.9
τ_g	0.95
f_p	0.9

5.2. Assembly the Aluminum Heat Sink to the Solar Panel Back Sheet

The aluminum heat sink is installed to the back sheet of the solar panel using a silicon thermal grease to fill any cavities. The objective of the aluminum heat sink is to reduce the adverse effects of any rise in temperature. The mechanical assembly is carried out by using screw bolts to ensure a tight contact between surfaces. Heat is dissipated by heat transfer and conduction from the solar panel back sheet to the surrounding air by convection and radiation as shown in Figure 7a and the thermal resistance diagram is shown in Figure 7b. As mentioned in [11], the thermal energy rating Q_r that results from the air touching the surfaces of the solar panel because of the resultant wind speed is given by Equation (45):

$$Q_r = m_A C_A (T_m - T_a) \tag{45}$$

The procedure is described by the flowchart depicted in Figure 7c.

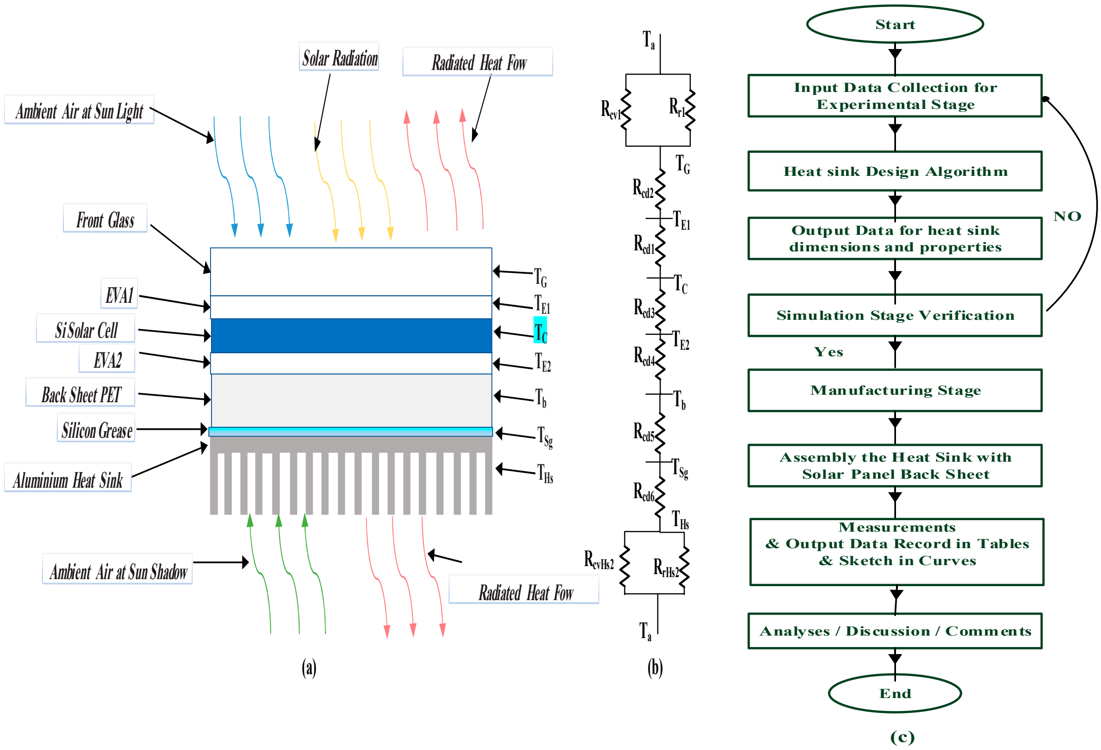

Figure 7. (**a**) Cross-section of the solar panel layers in conduction with aluminum heat sink, (**b**) Thermal resistance network of the solar panel layers, (**c**) Procedure description.

6. Simulation Model

The developed mathematical model is used to estimate the solar energy absorbed by the solar panel and perform the calculations of the temperatures of the solar cell, glass, and back sheet. Using this approach both the useful extracted electrical energy beside the thermal energy can also be calculated. The simulation model can be generated, for constant average ambient temperature and varying wind speeds when the average solar radiation is constant. The solar panel properties are given as in Table 2. The location coordinates of King Abdulaziz University (KAU) situated in Jeddah, Saudi Arabia, are detailed in Table 3. The parameters of the solar radiation S_r and the wind speed ω_s [59–61] were provided by the meteorological weather station as shown in Figure 8.

Table 3. Meteorological weather station parameters [21].

Weather Parameters	Values & Units
Latitude	21.49604°
Longitude	39.24492°
Elevation	75 m
S_r	672 W/m^2
ω_s	4–7 m/s
ω_t	0–11 m/s
ω_r	4–18 m/s
T_a	315 K

Table 4. Heat-sink selection parameters and properties.

Parameters of the Heat Sink	Values & Units
L	1646 mm
W	990 mm
H	40 mm
t_{bp}	0.5 mm
t_f	1.5 mm
d_f	25 mm
N	36
Material	Aluminum 6101-T6
Aluminum composition in Alloy	97%
Density	2.70 g/cc
Specific Heat Capacity	0.895 J/g-°C
Thermal Conductivity	239 W/m-K
Thermal resistance at natural convection	0.56 °C/W
Thermal resistance at forced convection	0.088 °C/W
Shear Strength	138 MPa
Ultimate Tensile Strength	221 MPa

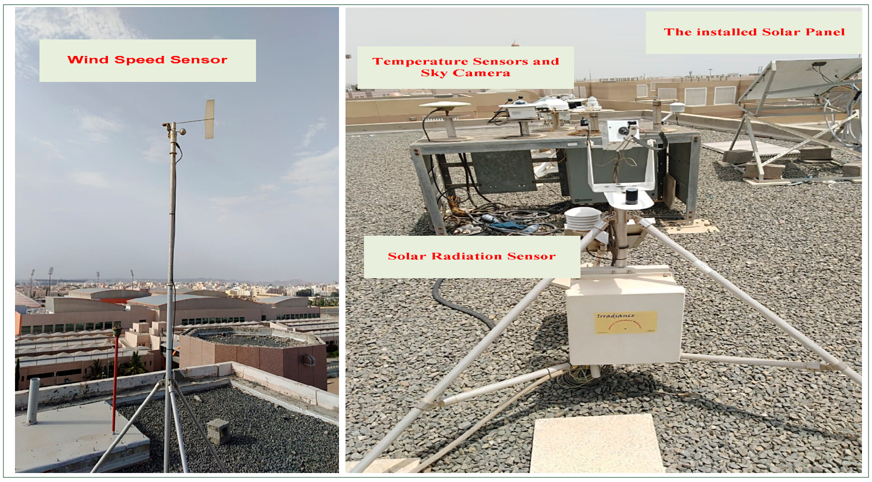

Figure 8. KAU meteorological weather station [21].

Simulation model is developed using computational program of MATLAB software, and simulation results are derived as follows:

6.1. Simulation of Solar Panel without a Heat Sink

This model describes the analysis of solar energy absorbed by the solar panel as shown in Figure 3. A computational MATLAB software program is run to calculate the temperatures of solar cells, glass, and back sheet as well as for calculating both the extracted electrical energy and the thermal energy including top, bottom and edge losses. The results are depicted in Tables 5–7 for various wind speeds (ω_r = 1–15 m/s).

Simulation results for the electrical characteristics without heat sink are presented in Table 8.

Table 5. Temperatures of layers at various wind speeds for the simulation model without heat sink (T_a = 315 K).

ω_r (m/s)	T_G (K)	T_{EVAg} (K)	T_C (K)	T_{EVAb} (K)	T_b (K)
1	338.88	340.69	341.11	340.69	339.50
2	327.76	329.09	329.39	329.07	328.15
3	323.68	324.82	325.08	324.79	323.96
4	321.51	322.54	322.78	322.51	321.73
5	320.16	321.12	321.33	321.07	320.32
6	319.23	320.13	320.33	320.08	319.35
7	318.55	319.40	319.59	319.34	318.63
8	318.04	318.84	319.02	318.78	318.07
9	317.63	318.39	318.57	318.32	317.63
10	317.29	318.03	318.20	317.96	317.26
11	317.02	317.73	317.89	317.65	316.96
12	316.79	317.47	317.63	317.39	316.70
13	316.60	317.25	317.40	317.16	316.48
14	316.43	317.06	317.21	316.97	316.29
15	316.28	316.89	317.03	316.79	316.12

Table 6. Heat transfer coefficients at varying wind speeds for the simulation model without heat sink.

ω_r (m/s)	h_w (W/m^2.K)	h_{rg} (W/m^2.K)	h_{rb} (W/m^2.K)	U_t (W/K)	U_b (W/m^2.K)	U_e (W/m^2.K)	η_{el}%
1	5.50	9.27	7.98	13.51	12.71	0.08	12.74
2	9.58	10.68	8.58	17.97	16.79	0.08	13.47
3	13.25	12.35	9.30	22.05	20.47	0.08	13.73
4	16.68	14.15	10.02	25.82	23.83	0.08	13.87
5	19.94	16.07	10.72	29.35	26.94	0.08	13.96
6	23.07	18.12	11.40	32.70	29.84	0.08	14.02
7	26.10	20.31	12.06	35.90	32.56	0.07	14.07
8	29.05	22.64	12.70	38.98	35.13	0.07	14.10
9	31.92	25.14	13.33	41.96	37.57	0.07	14.13
10	34.72	27.81	13.94	44.85	39.90	0.07	14.16
11	37.47	30.68	14.53	47.67	42.12	0.07	14.17
12	40.17	33.77	15.11	50.43	44.25	0.07	14.19
13	42.83	37.09	15.69	53.14	46.30	0.07	14.20
14	45.45	40.68	16.25	55.82	48.26	0.07	14.22
15	48.03	44.55	16.80	58.46	50.16	0.07	14.23

Table 7. Solar energy transmitted to the solar panel without heat sink (generated by the simulation model).

ω_r (m/s)	Q_{el} (W)	Q_t (W)	Q_b (W)	Q_e (W)	Q (W)
1	112.63	430.87	436.25	2.20	981.95
2	119.01	417.49	444.22	1.23	981.95
3	121.36	406.89	452.84	0.87	981.95
4	122.61	397.43	461.24	0.68	981.95
5	123.40	388.65	469.35	0.56	981.95
6	123.94	380.35	477.19	0.48	981.95
7	124.34	372.42	484.78	0.42	981.95
8	124.65	364.78	492.15	0.37	981.95
9	124.90	357.39	499.33	0.33	981.95
10	125.10	350.21	506.34	0.30	981.95
11	125.27	343.22	513.19	0.28	981.95
12	125.41	336.39	519.89	0.26	981.95
13	125.54	329.71	526.46	0.24	981.95
14	125.64	323.17	532.91	0.22	981.95
15	125.74	316.76	539.25	0.21	981.95

Table 8. Solar panel electrical characteristics without heat sink (generated using the simulation model).

ω_r (m/s)	V_{oc} (V)	V_{mpp} (V)	I_{sc} (A)	I_{mpp} (A)	P_{mpp} (W)	FF	η_{el}%
1	31.52	24.47	7.72	4.58	112.07	0.46	12.68
2	32.89	27.57	7.68	4.30	118.46	0.47	13.40
3	33.40	28.69	7.66	4.21	120.81	0.47	13.67
4	33.67	29.26	7.65	4.17	122.06	0.47	13.81
5	33.84	29.61	7.65	4.15	122.85	0.47	13.90
6	33.96	29.83	7.64	4.14	123.39	0.48	13.96
7	34.05	29.99	7.64	4.13	123.80	0.48	14.01
8	34.11	30.10	7.64	4.12	124.11	0.48	14.04
9	34.17	30.18	7.64	4.12	124.35	0.48	14.07
10	34.21	30.23	7.64	4.12	124.56	0.48	14.09
11	34.25	30.27	7.63	4.12	124.72	0.48	14.11
12	34.28	30.29	7.63	4.12	124.87	0.48	14.13
13	34.30	30.31	7.63	4.12	124.99	0.48	14.14
14	34.33	30.31	7.63	4.13	125.10	0.48	14.16
15	34.35	30.31	7.63	4.13	125.19	0.48	14.17

6.2. Simulation of Solar Panel with an Aluminum Heat Sink

This model describes the analysis of solar energy absorbed to the solar panel with the aluminum heat sink. The heat is dissipated by conduction with the solar panel back sheet via thermal grease, the properties of which are enumerated in Table 9. A computational MATLAB software program was run to calculate the temperatures of solar cell, glass, and back sheet. Also, both the salutary electrical energy and the thermal energy including top, bottom and edge losses were calculated by the same program.

The results are listed in Tables 10–12 for various wind speeds (ω_r = 1–15 m/s). The results indicate that the temperature of the solar cell is decreased and the heat transfer through the solar panel bottom is increased due to the installation of the aluminum heat sink. The more wind speed increases the more temperature decreases. Table 13 presents simulation results for the solar panel electrical characteristics with the aluminum heat sink. When wind speed increases, temperature decreases and therefore the electrical efficiency improves and the extracted power increases.

Table 9. Thermal grease properties.

Parameters of the Thermal Grease	Values & Units
Brand	GD380 Thermal Paste
Colour	Gray
Specific gravity	2.5 G/Cc
Thermal conductivity	2.2 W/m.K
Operating temperature	−50~200 °C

Table 10. Layers temperature at various wind speed for the simulation model with an aluminum heat sink (T_a = 315 K).

ω_r (m/s)	T_G (K)	T_{EVAg} (K)	T_C (K)	T_{EVAb} (K)	T_b (K)	T_{Hs} (K)
1	328.61	329.97	330.29	330.09	329.55	329.55
2	321.99	323.05	323.29	323.10	322.57	322.57
3	319.57	320.49	320.70	320.51	319.98	319.98
4	318.30	319.12	319.31	319.13	318.60	318.60
5	317.51	318.27	318.44	318.25	317.72	317.72
6	316.97	317.68	317.84	317.65	317.12	317.12
7	316.59	317.24	317.39	317.20	316.67	316.67
8	316.29	316.91	317.05	316.86	316.32	316.32
9	316.07	316.64	316.77	316.58	316.04	316.04
10	315.88	316.42	316.55	316.36	315.82	315.82
11	315.73	316.24	316.36	316.17	315.63	315.63
12	315.61	316.09	316.20	316.01	315.47	315.47
13	315.51	315.96	316.06	315.87	315.33	315.33
14	315.42	315.85	315.94	315.75	315.20	315.20
15	315.35	315.75	315.84	315.65	315.10	315.10

Table 11. Heat transfer coefficients at various wind speeds for the simulation model with aluminum heat sink.

ω_r (m/s)	h_w (W/m^2.K)	h_{rg} (W/m^2.K)	h_{rHs} (W/m^2.K)	U_t (W/K)	U_{Hs} (W/m^2.K)	U_e (W/m^2.K)	η_{el}%
1	9.06	10.47	0.89	17.39	9.48	0.08	13.41
2	15.78	13.66	1.03	24.82	15.51	0.08	13.84
3	21.82	17.28	1.16	31.37	20.62	0.08	14.00
4	27.47	21.36	1.28	37.34	25.15	0.07	14.09
5	32.84	25.99	1.40	42.91	29.24	0.07	14.14
6	37.99	31.25	1.50	48.20	33.00	0.07	14.18
7	42.98	37.28	1.61	53.29	36.48	0.07	14.21
8	47.82	44.24	1.71	58.25	39.73	0.07	14.23
9	52.55	52.31	1.81	63.13	42.77	0.07	14.24
10	57.17	61.76	1.90	67.97	45.64	0.07	14.26
11	61.70	72.94	1.99	72.82	48.35	0.07	14.27
12	66.15	86.32	2.08	77.74	50.92	0.07	14.28
13	70.52	102.56	2.17	82.77	53.36	0.07	14.29
14	74.83	122.62	2.25	87.96	55.69	0.07	14.29
15	79.08	147.93	2.33	93.37	57.92	0.07	14.30

Table 12. Solar energy transmitted to the solar panel with aluminum heat sink (generated from the simulation model).

ω_r (m/s)	Q_{el} (W)	Q_t (W)	Q_{Hs} (W)	Q_e (W)	Q (W)
1	118.52	252.90	609.22	1.31	981.95
2	122.33	213.30	645.60	0.73	981.95
3	123.74	192.10	665.61	0.51	981.95
4	124.50	176.92	680.14	0.40	981.95
5	124.97	164.72	691.94	0.33	981.95
6	125.30	154.33	702.05	0.28	981.95
7	125.54	145.17	711.00	0.24	981.95
8	125.73	136.92	719.09	0.21	981.95
9	125.88	129.38	726.50	0.19	981.95
10	126.00	122.41	733.37	0.18	981.95
11	126.10	115.91	739.77	0.16	981.95
12	126.19	109.83	745.79	0.15	981.95
13	126.27	104.09	751.45	0.14	981.95
14	126.33	98.67	756.82	0.13	981.95
15	126.39	93.52	761.92	0.12	981.95

Table 13. Electrical characteristics of the solar panel for the simulation model with aluminum heat sink.

ω_r (m/s)	V_{oc} (V)	V_{mpp} (V)	I_{sc} (A)	I_{mpp} (A)	P_{mpp} (W)	FF	η_{el}%
1	32.91	27.65	7.67	4.29	118.52	0.47	13.41
2	33.73	29.48	7.65	4.15	122.33	0.47	13.84
3	34.03	30.13	7.64	4.11	123.74	0.48	14.00
4	34.20	30.46	7.64	4.09	124.50	0.48	14.09
5	34.30	30.65	7.63	4.08	124.97	0.48	14.14
6	34.37	30.77	7.63	4.07	125.30	0.48	14.18
7	34.42	30.85	7.63	4.07	125.54	0.48	14.21
8	34.46	30.90	7.63	4.07	125.73	0.48	14.23
9	34.50	30.93	7.63	4.07	125.88	0.48	14.24
10	34.52	30.94	7.63	4.07	126.00	0.48	14.26
11	34.54	30.95	7.63	4.07	126.10	0.48	14.27
12	34.56	30.95	7.62	4.08	126.19	0.48	14.28
13	34.58	30.94	7.62	4.08	126.27	0.48	14.29
14	34.59	30.92	7.62	4.09	126.33	0.48	14.29
15	34.60	30.90	7.62	4.09	126.39	0.48	14.30

6.3. Comparison of Results of the Two Simulation Models

This section discusses the comparison of results of the two simulation models, without heat sink and with aluminum heat sink. The aluminum heat sink which is installed to the solar panel back sheet via thermal grease improves the thermal conductivity and appears to be effective at lowering the temperature. The aluminum heat sink causes a decrease in the thermal resistance of the bottom surface of the solar panel, which is equal to the inverse value of the heat transfer coefficient. When the aluminum heat sink is installed, the heat transfer through the bottom surface is increased, as shown in Figures 9 and 10, leading to a decrease in the solar cell temperature for similar weather conditions and wind speed where the the thermal losses are decreased and the extracted power is increased. The average ambient temperature is (T_a = 315 K) for this research, and the location is Jeddah, the coordinates for which have been given in Table 3. Jeddah is situated near the Equator and has hot weather during most parts of the year. The aluminum heat sink installation reduces the solar cell temperature which enhances the solar panel electrical characteristics. Thanks to the aluminum heat sink, the temperature and the thermal losses are decreased and the resulting average voltage drop is also decreased, then the solar panel open circuit and the MPP voltages V_{oc} and V_{mpp} are increased as shown in Figure 11. Also, the solar panel short circuit and the MPP currents I_{sc} and I_{mpp} are increased as shown in Figure 12. Consequently, the maximum power point is increased and the accumulative energy per day is increased.

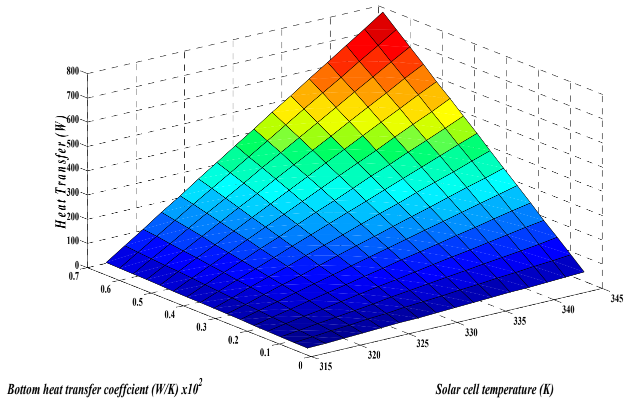

Figure 9. Increase in bottom heat transfer with solar cell temperature reduction due to installation of the aluminum heat sink.

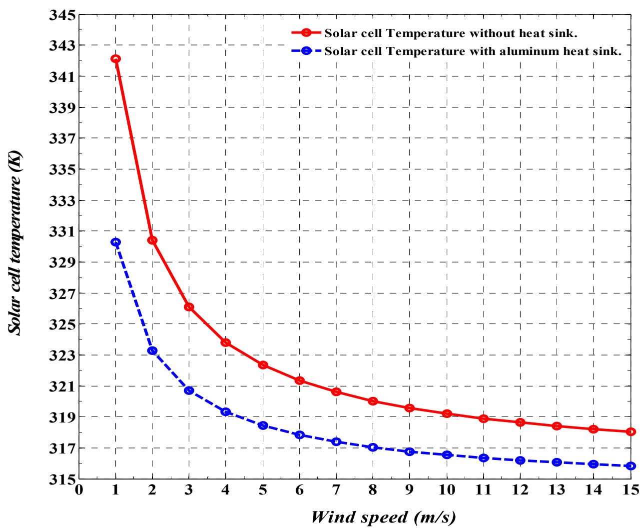

Figure 10. Solar cell temperature for various wind speeds with and without installation of the aluminum heat sink.

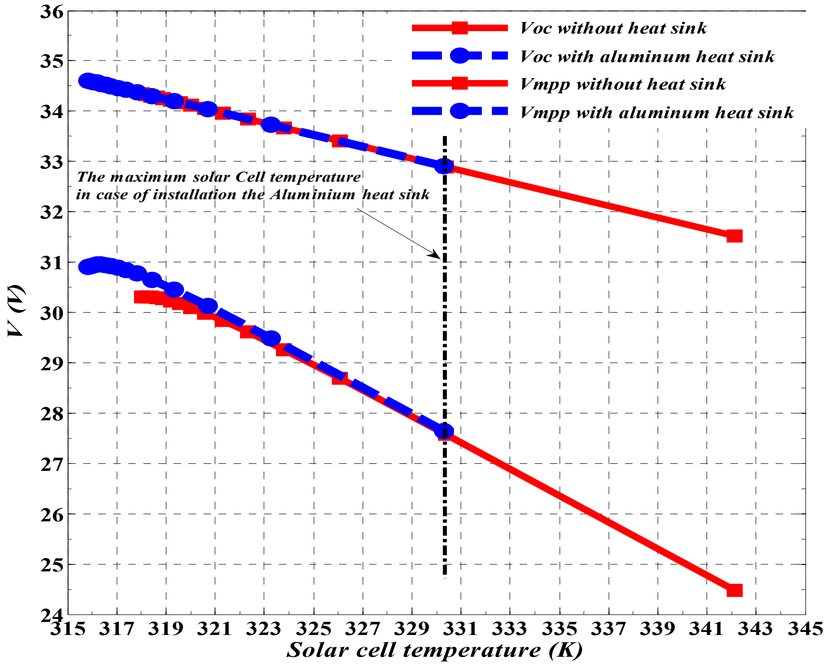

Figure 11. Electrical parameters of the solar cell: Open circuit voltage and MPP voltage variations at different solar cell temperatures.

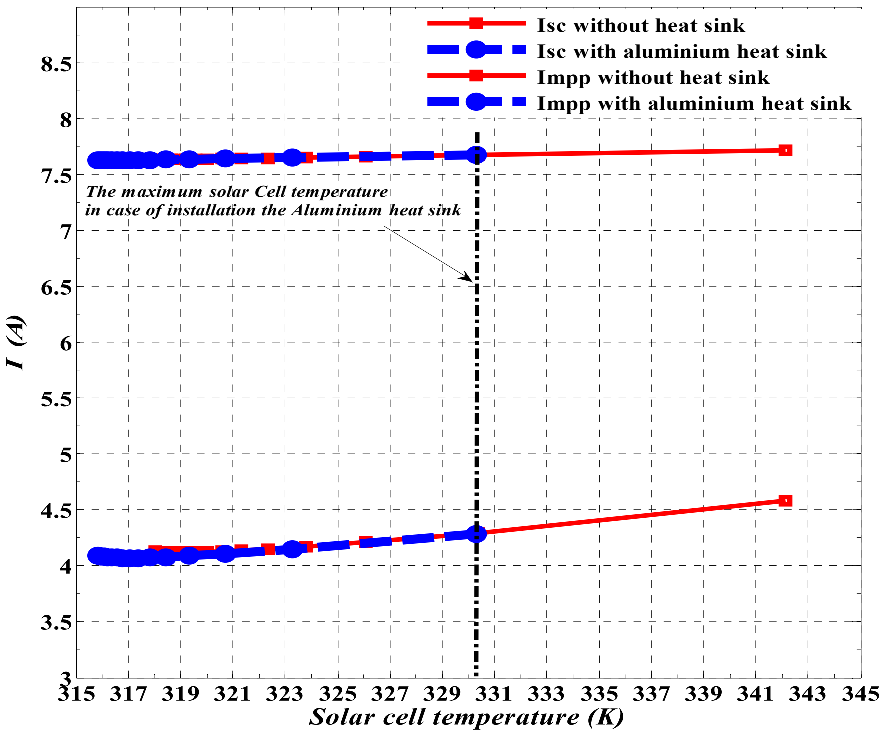

Figure 12. Electrical parameters of the solar cell: Short circuit current and MPP current at different solar cell temperatures.

It is clear that reduction in the solar cell temperature reduction has enhanced the electrical efficiency. This results are shown in Figure 13. Also, Figure 14 indicates that solar panel maximum output power is also increased.

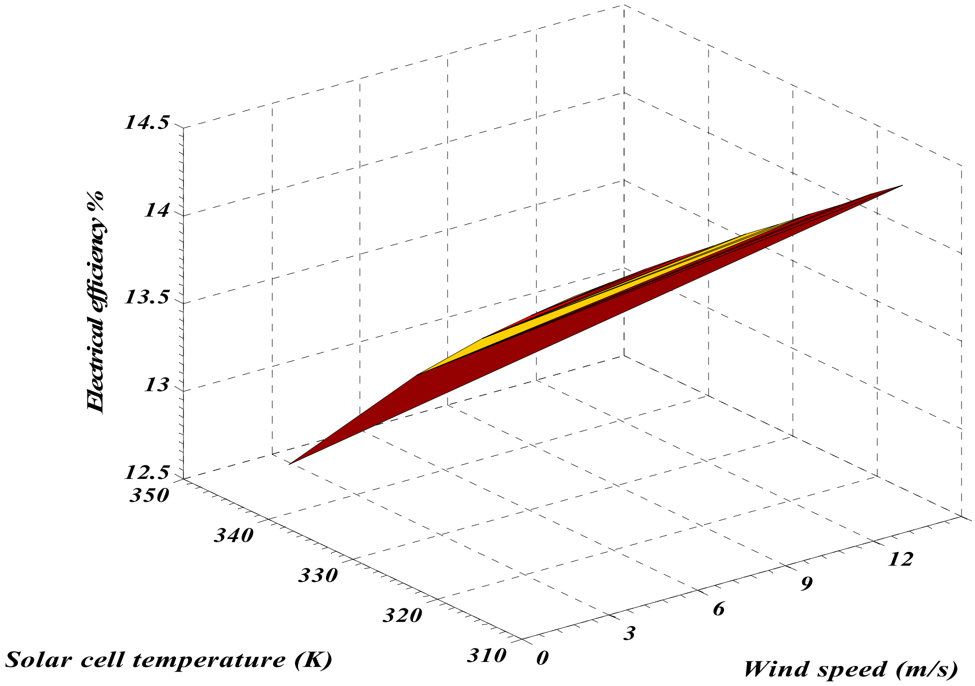

Figure 13. Three-dimentional graph of the solar panel perforamce: Efficiency, temperature and wind speeds.

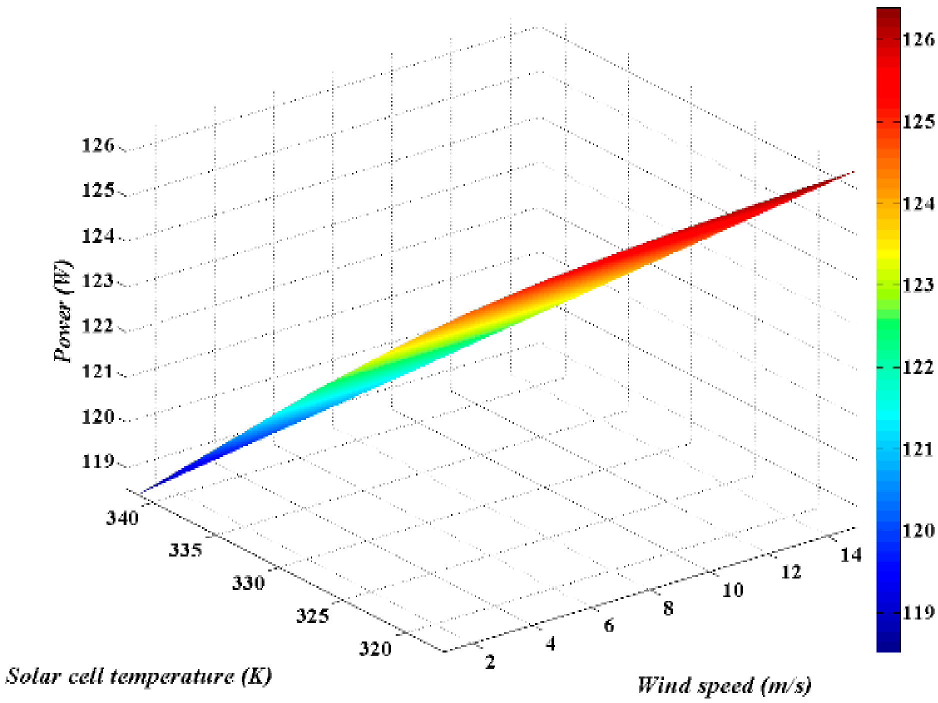

Figure 14. Three-dimentional graph of the solar panel perforamce: Output power at different temperature and wind speeds.

7. The Experimental Setup Models

The experimental setup model is implemented as per the schematic diagram shown in Figure 15. This setup uses a 250-Watt solar panel to charge 200 Ah deep cycle gel battery via 30 A *MPPT* solar charger controller. The battery is used to energize a 84-watt street lighting fixture. As per the Saudi Arabian General Authority of Meteorology and Environmental Protection [62], as well as the data obtained from King Abdulaziz University (KAU) weather station, which is shown in Figure 8, the highest ambient temperature is observed during summer season in June, so this study was conducted under June climatic conditions to study the effect of maximum temperature on the solar panel performance. The solar panel was installed at a fixed tilt angle (θ = 25°), orientation south, sloped by azimuth angle (ϕ = 10°) towards the west direction. The details of the set up as well as the results are presented as follows.

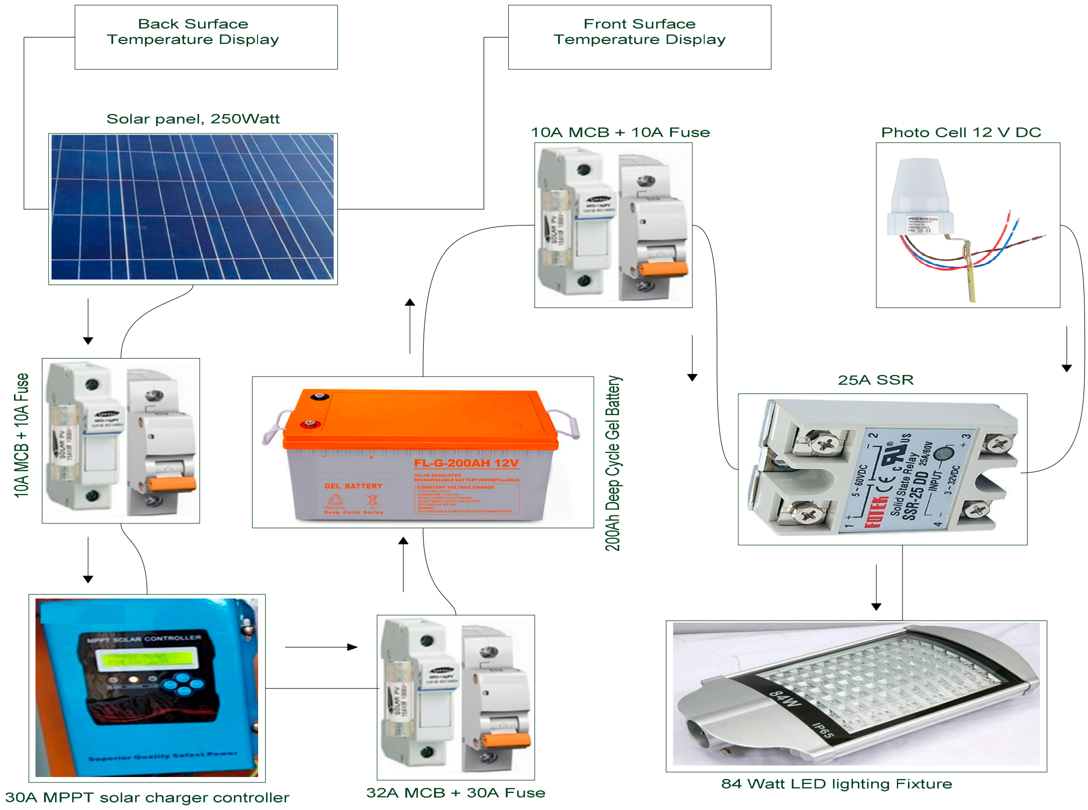

Figure 15. Schematic diagram of the experimental model implementation.

7.1. The Experimental Setup Model without Heat Sink

This case elaborates the effect of temperature on the solar panel performance without using the heat sink as detailed in Figure 3. The average readings during daylight hours in June are presented in Table 14, where T_a is the average ambient temperature, T_{SFS} is the solar panel front surface temperature, and T_{SBS} is the temperature of the solar panel back surface.

Table 14. Readings without a heat sink.

Time (h)	T_a (°C)	T_{SFS} (°C)	T_{SBS} (°C)	V_{oc} (V)	V_{mpp} (V)	I_{mpp} (A)	P_{mpp} (W)
05:30 a.m.	28	28	28	21.1	21.1	0.05	1
06:00 a.m.	28.5	29	28.8	28.2	17.7	0.4	7
06:30 a.m.	28.5	29.6	29.4	29.9	17.9	0.5	8
07:00 a.m.	29	31	30.3	31.3	21.2	0.7	14
07:30 a.m.	30.5	33.4	32.6	32.3	24.5	1.1	25
08:00 a.m.	32.5	33.5	33	32.8	23.6	1.8	40
08:30 a.m.	34.5	38	37	33	23	2.3	50
09:00 a.m.	37	41.2	39.6	32.8	21.6	3.2	64
09:30 a.m.	38	43.5	42	31.7	21	3.6	73

Table 14. *Cont.*

Time (h)	T_a (°C)	T_{SFS} (°C)	T_{SBS} (°C)	V_{oc} (V)	V_{mpp} (V)	I_{mpp} (A)	P_{mpp} (W)
10:00 a.m.	38.5	44	42.5	30.6	20.9	3.9	78
10:30 a.m.	39	46.1	44.6	30.4	20.3	4.4	86
11:00 a.m.	39.5	48	46	30.2	20	4.9	96
11:30 a.m.	40	49.3	47	30	18.7	5.4	99
12:00 p.m.	41	49.5	47.2	29.8	18.3	5.6	100
12:30 p.m.	41.3	49.6	47.3	29.6	18	5.8	103
01:00 p.m.	41.6	49.7	47.5	29.4	17.6	6	101
01:30 p.m.	41.8	50.1	48	29	17.5	5.9	98
02:00 p.m.	42.4	50.9	48.7	28.4	17.4	5.8	94
02:30 p.m.	42	50.2	48.5	28.6	17.1	5.7	93
03:00 p.m.	40.2	49	47	29.6	18.8	5	89
03:30 p.m.	40.5	48	46.5	30.2	20.1	4.2	80
04:00 p.m.	39.5	46.5	45.2	31	21.6	3.4	70
04:30 p.m.	39	45	43.6	31.4	22.4	2.7	56
05:00 p.m.	38.5	43	41.5	31.8	22.8	1.8	37
05:30 p.m.	38	42	41	32	18.6	1.4	20
06:00 p.m.	37	40.5	36.5	28.5	17.8	0.34	5
06:30 p.m.	35.2	38	35.5	26.4	0	0	0
07:00 p.m.	31	32	30.5	24	0	0	0
07:30 p.m.	28	30	30	1.5	0	0	0
08:00 p.m.	28	28.5	28.5	1.5	0	0	0

7.2. The Experimental Setup Model with an Aluminum Heat Sink

This case studied the effect of temperature on the solar panel performance using the aluminum heat sink as detailed in Figure 7. The average readings during daylight hours in June are presented in Table 15, where T_{HSS} is the heat sink outlet surface temperature.

Table 15. Experimental readings with an aluminum heat sink.

Time (hr.)	T_a (°C)	T_{SFS} (°C)	T_{HSS} (°C)	V_{oc} (V)	V_{mpp} (V)	I_{mpp} (A)	P_{mpp} (W)
05:30 a.m.	28	28	28	21.1	21.1	0.04	1
06:00 a.m.	28.5	29	28.5	28.2	17.3	0.36	7
06:30 a.m.	28.5	29.6	29.4	29.9	17.9	0.4	8
07:00 a.m.	29	30.8	29.8	31.3	21.2	0.72	18
07:30 a.m.	30.5	33	31	32.3	26.7	1.24	32
08:00 a.m.	32.5	33.5	32.7	33.8	26.7	1.85	48
08:30 a.m.	34.5	37	35	34.5	26.5	2.45	60
09:00 a.m.	37	40	38	34.2	26	3.1	78
09:30 a.m.	38	42.5	39	33.8	25.6	3.4	85
10:00 a.m.	38.5	43	39.5	33.7	25.2	3.7	90
10:30 a.m.	39	44.1	39.8	33.4	25	4	96
11:00 a.m.	39.5	47	40.2	33.2	24	4.4	102
11:30 a.m.	40	47.3	40.8	33	22	5	104
12:00 p.m.	41	47.5	41.5	32.8	21.8	5.1	105
12:30 p.m.	41.3	47.6	41.8	32.6	21.4	5.2	107
01:00 p.m.	41.6	47.6	42	32.4	20.4	5.5	108
01:30 p.m.	41.8	48	42.2	31	20	5.6	103
02:00 p.m.	42.4	48.2	42.6	30.8	20	5.5	102
02:30 p.m.	42	47.8	42.4	30.6	19.8	5.5	99
03:00 p.m.	40.2	47	40.5	30.4	19.4	5	92
03:30 p.m.	40.5	45.5	40.2	30.2	22.8	4	86
04:00 p.m.	39.5	44	40	32.5	22.4	3.8	80
04:30 p.m.	39	43	40	32.8	22.2	3.4	70
05:00 p.m.	38.5	42.6	39.6	33.8	22	2.72	56
05:30 p.m.	38	42	38.5	34	18.8	1.92	32
06:00 p.m.	37	40.5	37.8	29.5	18.5	1.2	20
06:30 p.m.	35.2	38	35.5	28.5	17.8	0.52	8
07:00 p.m.	31	35	31	26	0	0	0
07:30 p.m.	28	30	28	1.5	0	0	0
08:00 p.m.	28	28	28	1.5	0	0	0

7.3. Comparison and Comments

This section discusses the comparison of the results of the two experimental setup models, with and without the aluminum heat sink. The comparison at this stage is limited to the solar panel electrical characteristics at variable ambient temperatures during different parts of the day, as shown in Figure 16. The maximum solar panel front surface temperature without cooling is 50.8 °C and it dropped to 48.2 °C for the same time of the day (2:00 p.m.) when the aluminum heat sink was used- a drop of about 3.7%. When the maximum solar panel back surface temperature without cooling was 48.5 °C, it dropped to 42.4 °C for the same time (2:30 p.m.) when the heat sink was used- a decrease of 14.3%. Results of the experiment for the solar panel output voltage, current, and power are plotted with ambient temperature as shown in Figures 17–19, respectively. The maximum open circuit voltage $V_{oc}(V)$ without heat sink is recorded as 33 V at 8:30 a.m. while this value is 34.5 V (at 8:30 a.m.) when the heat sink is used—an increase of about 4.5%. Moreover, maximum power point voltage V_{mpp} is changed from 24.5 to 26.7 V at 7:30 a.m. when a heat sink is used-an increase of 9%. The maximum power point current I_{mpp} is recorded as 6 A without heat sink while it was 6.5 A when heat sink was used, time being constant at 1:00 p.m.—a decrease of 6.67%. From the results of this experiment, it can be concluded that the electrical characteristics of the solar panel are enhanced when aluminum heat sink is used. This is because of a decrease in the solar cell temperature leading to a rise in the open circuit voltage as well as the maximum power voltage. There is a slight decrease in output current due to the fall in temperature as shown in Figures 17 and 18, respectively. The output power is increased and the electrical energy generated by the solar panel is increased as shown in Figure 19. Values for all points are increased—for example at 9 a.m. the power increased from 63 to 79 which is a 25.4% increase at an ambient temperature of 37 °C. As a result of the increase in solar panel output power throughout the daylight hours, the output energy increased from 1587 watt/day to 1797 watt/day amounting to a 13.23% increase overall. The insertion of aluminum heat sink to the solar panel decreases the solar cell temperature and limits the hot spot phenomena, which increases the life of the unit. Figure 20 shows the thermal images of solar panel surfaces with and without aluminum heat sink.

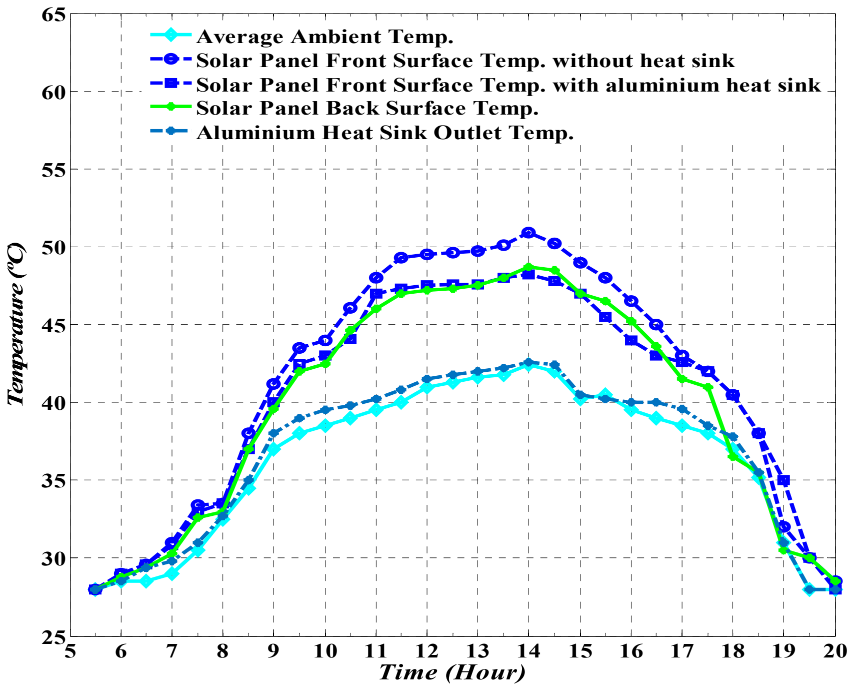

Figure 16. Temperatures curves of the solar panel experimental model.

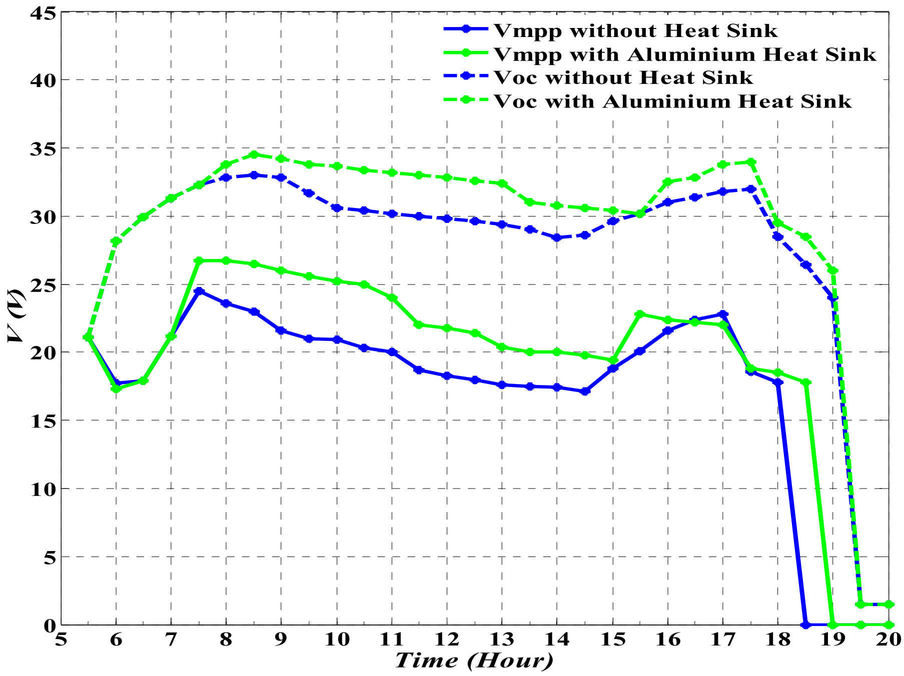

Figure 17. Output voltage curves of the solar panel experimental model.

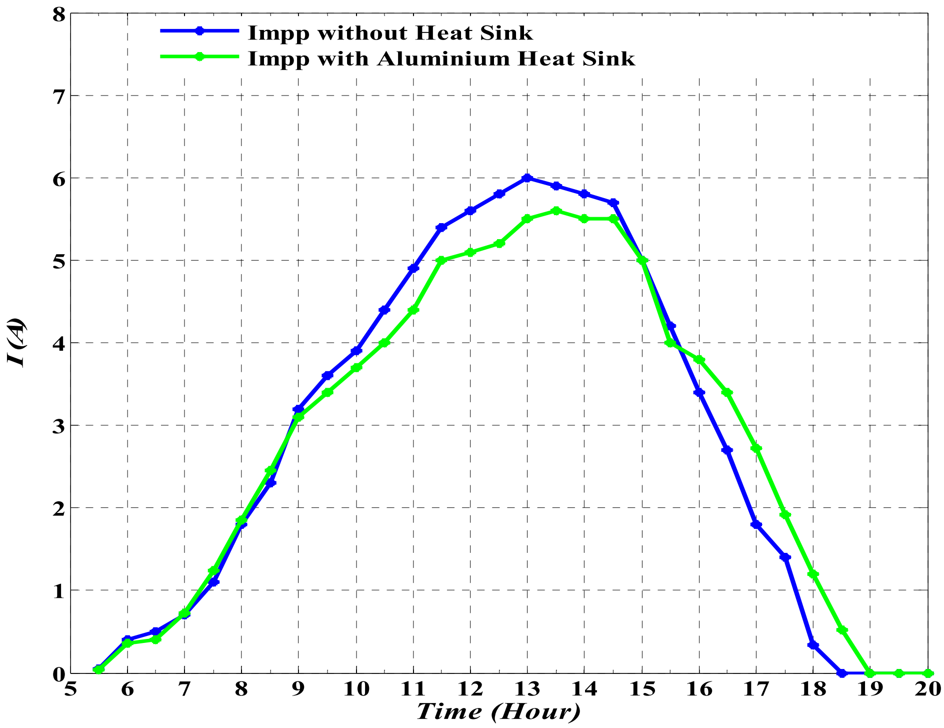

Figure 18. Output current curves of the solar panel experimental model.

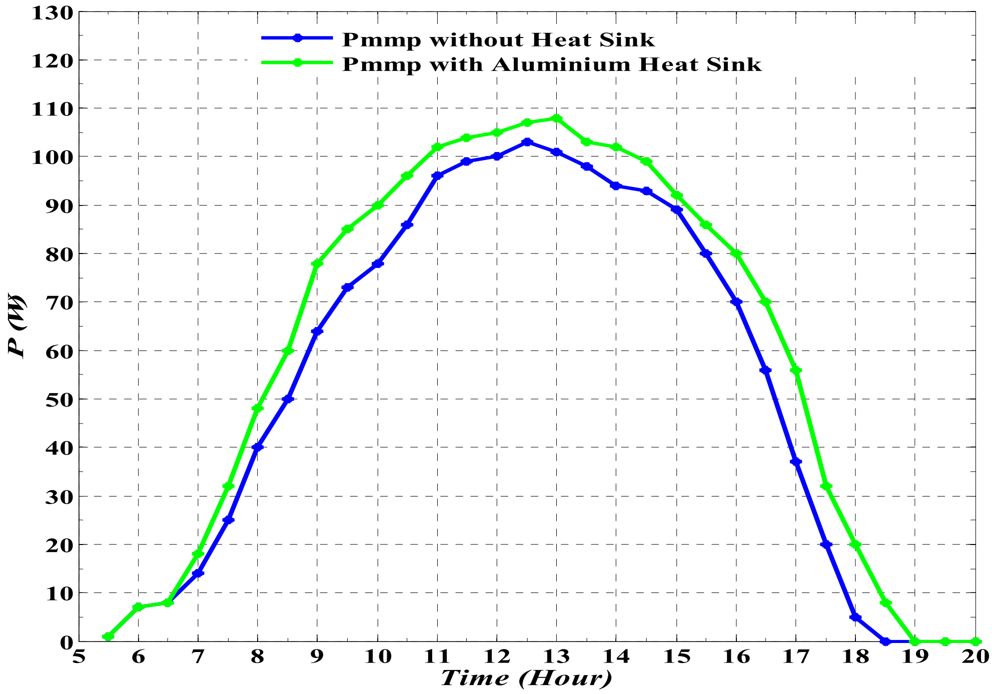

Figure 19. The output power curves of solar panel experimental model.

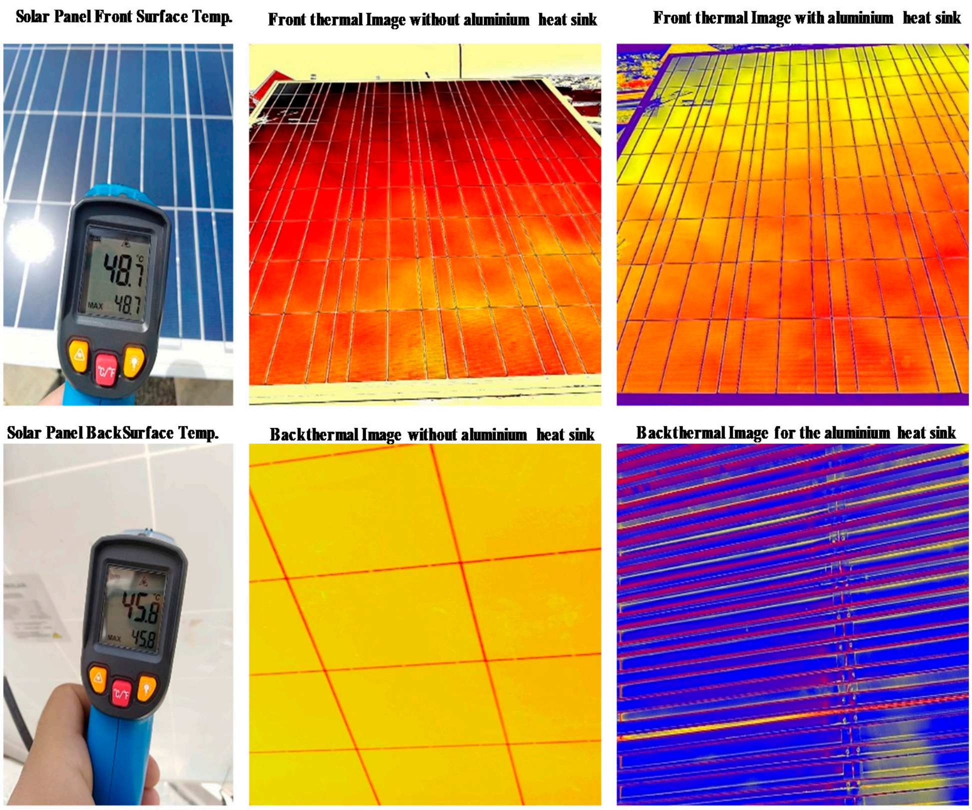

Figure 20. Thermal images of the solar panel surfaces without and with the aluminum heat sink.

8. Conclusions

This paper discussed steady state heat transfer through solar panel layers and studied the effect of high temperatures on the solar panel performance in a hot desert environment with varying wind speed. In our simulation it has been found that the solar cell temperature is decreased when an aluminum heat sink is installed. The total thermal resistance is decreased due to the high thermal conductivity and large surface area of the aluminum heat sink due to its fins. Subsequently, there is acceleration of heat transfer through the solar panel back surface leading to a decrease of 11 °C in the solar cell temperature. In the experimental stage, it was concluded that the installation of aluminum heat sink on the solar panel back surface leads to a decrease in the solar cell temperature by 16.4%, which leads to an enhancement of the electrical characteristics in the form of increase in both the open circuit voltage and maximum power point voltage. It also produces a slight reduction in the maximum power point current. In the experimental stage, the overall extracted electrical energy from the solar panel with aluminum heat sink is increased by more than 13.23% per day when compared with the case when no such a heat sink was not used. This validates the theoretical and simulation studies that have shown that the heat sink installation effectively mitigates the temperature negative effect and enhances the solar panel electrical performance.

Therefore, this paper concludes that the installation of the aluminum heat sink on the back surface of solar panels leads to a mitigation of the solar cell temperature and limits the hot spot phenomena. It also enhances the electrical characteristics and increases both solar panel efficiency and lifetime.

Author Contributions: Y.H. did the experimental work and reported the results, shared the analysis and writing of the manuscript. M.A.I. guided the proposed electrical design, in addition to the editing and review of the written manuscript, O.M.A.-R. and B.A.H. strategy proposed and guided the mechanical design of the heat think. and contribute to the manuscript writing. M.O., A.A. and A.E.A. was responsible for the guidance and a number of key suggestions in addition to the editing and review of the written manuscript. All authors have read and agreed to the published version of the manuscript.

Funding: This research was co-funded by the Renewable Energy & Smart Grid Lab (RESGL), Electrical Engineering and Computer Department, KAU by providing facilities and support. Y. Hassan and M. Orabi would also like to express our gratitude for Aswan Power Electronic Applications Research Center (APEARC), Aswan University for their immense support under STDF grant ID: 15261. Abdelali El Aroudi would like to thank the Spanish Agencia Estatal de Investigación (AEI) and the Fondo Europeo de Desarrollo Regional (FEDER) under grant DPI2017-84572-C2-1-R (AEI/FEDER, UE).

Acknowledgments: The authors would like to thank. Gulf Lighting Company helped us the manufacture of the aluminum heat sink which we used in our experiments, for which we are thankful to them.

Conflicts of Interest: The authors declare no conflict of interest.

Nomenclature

Q_C	Amount of energy inherited through the glass surface (Joule or W.h).	R_c	Contact thermal resistance (°C/W).
Q_{el}	Useful energy is converted to electrical energy (Joule or W.h).	R_{Hs}	Lumped heat sink thermal resistance (°C/W).
Q_{th}	Thermal energy losses (Joule or W.h).	R_{fin}	Fins thermal resistance (°C/W).
Q_{fT}	Total heat transfer rate from the heat sink surface (Joule or W.h).	R_{fins}	Lumped thermal resistance of total number of fins (°C/W).
Q_{fins}	Heat transfer rate from the heat sink fins surface (Joule or W.h).	R_{fa}	Thermal resistance of the ambient air through the film (°C/W).
Q_{unfins}	Heat transfer rate from the heat sink unfins surface (Joule or W.h).	R_{bpb}	Thermal resistance of the back heat sink base plate (°C/W).
Q_r	Thermal energy rating that results from the air touching surfaces (Joule or W.h).	R_{inr}	Interface thermal denoted (°C/W).
α_C	Cell absorptivity.	R_{sp}	Heat sink spread thermal resistance (°C/W).
λ	Thermal diffusivity (= 2.84×10^{-5} m^2/s).	R_{cd}	Conduction thermal network resistance (°C/W).
τ_g	Glass transmissivity.	R_{cv}	Convection thermal network resistances (°C/W).
q	Electron charge (= 1.602×10^{-19} C).	R_r	Radiation thermal network resistance (°C/W).

ψ_{av}	Dimensionless spreading resistance
S_r	Solar radiation (W/m^2).
f_p	Packing factor that refers to the area filled with solar cells from the total surface area.
FF	Fill factor.
g	Gravitational constant (= 9.81 m/s^2).
A	Surface area (m^2).
A_e	Edge area (m^2).
A_f	Fin cross-sectional area (m^2).
A_{fv}	Vehicle front area (m^2).
A_{fins}	Fins area of the heat sink (m^2).
A_{unfins}	Total unfins area of the heat sink (m^2).
H	Heat sink height (m).
W	Heat sink width (m).
d_f	Spacing between two consequential fins (m).
η_{el}	Eelectrical efficiency.
η_o	Nominal electrical efficiency
η_{th}	Thermal efficiency.
η_{fins}	Efficiency of heat sink fins.
β	Temperature coefficient that relies on the material type (K^{-1}).
T_o	Solar cell temperature at the () Standard Test Conditions (°C or K).
T_a	Average ambient temperature (°C or K).
T_C	Solar cell temperature at the operating conditions (°C or K).
T_G	Glass temperature (°C or K).
T_b	Back sheet temperature (°C or K).
T_c*	Cell temperature when the efficiency Approaching to zero (°C or K).
T_s	Sky temperature (°C or K).
T_{Hs}	Temperature of heat sink surface (°C or K).
T_m	Mean absorbed cell temperature (°C or K).
δ	Volumetric coefficient of expansion (K^{-1})
a	Diode ideality factor ($1 \le a \le 2$).
ρ	Density of the air (= 1.225 kg/m^3).
P_{mpp}	Output power (W) that is tracked at the Maximum Power Point (MPP).
V_{mpp}	Voltage of the *PV* source at the MPP (V).
V_{OC}	Voltage of the *PV* source at open circuit (V).
V_{pv}	PV output voltage (V).
V_T	Thermal voltage (V).
V_d	Diode voltage (V).
I_{mpp}	Current of the *PV* source at the *MPP* (A).
I_{SC}	Current of the *PV* source at short circuit (A).
I_{pv}	PV output current (A).
I_d	Diode current (A).
I_L	Light current (A).
I_o	Reverse saturation current (A).
m_A	Air mass flow rate.
ζ	Reflection coefficient of the glass = 0.1.
R_s	Series resistance of single diode solar cell (Ω).
R_{sh}	Shunt resistance of single diode solar cell (Ω).
k_e	Thermal conductivity of the edge insulation [W/(m.K)].
k	Thermal conductivity [W/(m.K)].
k_a	Thermal conductivity of the air (= 0.0291 [W/(m.K)]).
K_r	Interface thermal conductivity [W/(m.K)].
K_{BZ}	Boltzmann constant (= 1.3807 × 10^{-23} J/K).
U_L	Overall heat transfer coefficient.
U_t	Heat transfer coefficients of top.
U_b	Heat transfer coefficients of the bottom.
U_e	Heat transfer coefficients of the edges.
t	Thickness of any solar panel layer (mm).
t_{bp}	Thickness of heat sink base plate (mm).
t_f	Thickness of heat sink fin (mm).
t_e	Edge insulation thickness (mm).
h_r	Everall heat transfer coefficient.
h_r	Radiation heat transfer coefficient.
h_{cv}	Convection heat transfer coefficient.
h_c	Surrounding air heat transfer coefficient due to convection
h_w	Convective heat transfer coefficient due to wind speed.
C_A	Air specific heat
C_D	Coefficient of aerodynamic drag which depends on vehicle brand and is in the range of 0.297.
C_g	Constant = 2.677 × 10^4 for silicon.
c_e	Empirical constant in the range of 0.593.
E_g	Bandgap energy that relies on the material type, E_{go} = 1.12 eV or 1.794 × 10^{-19} J.
ε_r	Material emissivity of heat sink.
ε	Emissivity coefficient of any solar panel layer.
μ	Kinematic viscosity of the air (= 1.96 × 10^{-5} m^2/s).
σ	Porosity hole area to solar panel area (= 5.67 × 10^{-8} J/K)
p	Perimeter of solar panel (m).
p_f	Fin perimeter (m).
ω_r	Resultant wind speed due to natural air and turbulence air (m/s).
ω_s	Wind speed of natural air (m/s).
ω_t	Wind speed of turbulence air (m/s).
ω_v	Vehicle average speed (m/s).
L_v	The scaled turbulence motion length (m).
L_{ch}	Surface characteristic length of solar panel (m).
n_v	Vehicles number per unit length.
N_f	Total number of fins.
Nu	Nusselt number.
Re	Reynold number.
Pr	Prandtl number.
Ra	Rayleigh number.
G_r	Grashoff number.

Appendix A

The mathematical model of a single diode solar cell electrical model is described (as shown in Figure 5) for a solar panel that consists of n_c solar cells. The open circuit voltage is denoted by V_{oc}. The short circuit current is I_{sc}, while V_{pv}, and I_{pv} are the output voltage and current. I_L is the light current, I_o is the reverse saturation current, while V_d and I_d are the diode voltage and current respectively. All these parameters rely on the thermal voltage V_T that depends on the solar cell temperature [24,30,31,47–49], where ($1 \leq a \leq 2$) is the diode ideality factor, ($K_{BZ} = 1.3807 \times 10^{-23}$ J/K) is the Boltzmann constant, ($q = 1.602 \times 10^{-19}$ C) is the electron charge. The electrical performance is described as per the following equations:

$$V_T = \frac{aK_{BZ}T_C}{q} \tag{A1}$$

$$V_{oc} = V_T \ln\left(\frac{I_{sc}}{I_o} + 1\right) \tag{A2}$$

$$I_{sc} = I_L - I_o\left(e^{\frac{I_{sc}R_s}{V_T}} - 1\right) - \frac{I_{sc}R_s}{R_{sh}} \tag{A3}$$

$$I_L = I_{sc}e^{\frac{V_{oc}}{V_T}}\left(e^{\frac{V_{oc}}{V_T}} - 1\right) - \frac{V_{oc}}{R_{sh}} \tag{A4}$$

$$I_o = I_{sc}e^{\left(\frac{V_{oc}}{V_T} + \frac{E_{go}}{K_{BZ}T_o} - \frac{E_g}{K_{BZ}T_C}\right)} \tag{A5}$$

$$\frac{E_g}{E_{go}} = 1 - C_g(T_C - T_o) \tag{A6}$$

$$V_d = V_T \ln\left(\frac{I_d}{I_o} + 1\right) \tag{A7}$$

$$I_d = I_o\left(e^{\frac{V_d}{V_T}} - 1\right) \tag{A8}$$

$$V_{pv} = n_c\left(V_d - I_{pv}R_s\right) \tag{A9}$$

$$I_{pv} = I_{sc} - I_o\left(e^{\frac{(V_{pv}+I_{pv}R_s)}{V_T}} - 1\right) - \frac{V_{pv} + I_{pv}R_s}{R_{sh}} \tag{A10}$$

where E_g is the bandgap energy that relies on the material type, $E_{go} = 1.12$ eV or 1.794×10^{-19} J and the constant $C_g = 2.677 \times 10^4$ for silicon. The output power P_{mpp} at the MPP is given in Equation (6). There are many methods to calculate the Voltage V_{mpp} and current I_{mpp} at the MPP, as mentioned in [31], by differentiation of the output power $P = VI$ with respect to the voltage V that is given in Equation (A11). The current I_{mpp} at the MPP is given by Equation (A12), then V_{mpp} and I_{mpp} are given by simultaneously numerical solution for Equations (A11) and (A12):

$$\frac{I_{mpp}}{V_{mpp}} = \frac{\frac{I_o}{V_T}e^{\frac{(V_{mpp}+I_{mpp}R_s)}{V_T}} + \frac{1}{R_{sh}}}{1 + \frac{R_s}{R_{sh}} + \frac{I_oR_s}{V_T}e^{\frac{(V_{mpp}+I_{mpp}R_s)}{V_T}}} \tag{A11}$$

$$I_{mpp} = I_L - I_o\left(e^{\frac{(V_{mpp}+I_{mpp}R_s)}{V_T}} - 1\right) - \frac{V_{mpp} + I_{mpp}R_s}{R_{sh}} \tag{A12}$$

Another method to calculate V_{mpp} and I_{mpp} [50], where V_{mpp} is given as in Equations (A13) and (A14) respectively:

$$V_{mpp} = V_T \ln\left(\frac{I_{sc} - I_{mpp}}{I_o} + 1\right) - I_{mpp}R_s \tag{A13}$$

$$I_{mpp} + \frac{\left(I_{mpp} - I_{sc} - I_o\right)\left[\ln\left(\frac{I_{sc}-I_{mpp}}{I_o} + 1\right) - \frac{I_{mpp}R_s}{V_T}\right]}{1 + \left(I_{mpp} - I_{sc} - I_o\right)\frac{R_s}{V_T}} = 0 \tag{A14}$$

where I_{mpp} can be calculated starting from an initial guess and using numerical root-finding algortigms such as those implemented in *fsolve or fzero* functions of the MATLAB software. Then, the resulting value of I_{mpp} can be substituted in Equation (A14) to get V_{mpp}.

References

1. Salam, M.A.; Khan, S. Transition towards sustainable energy production—A review of the progress for solar energy in Saudi Arabia. *Energy Explor. Exploit.* **2017**, *36*, 3–27. [CrossRef]
2. El-Sebaii, A.A.; Al-Agel, F. Estimation of horizontal diffuse solar radiation from common meteorological parameters: A case study for Jeddah, Saudi Arabia. *Int. J. Ambient. Energy* **2013**, *34*, 92–99. [CrossRef]
3. Ahmad, N.I.; Kadir, M.Z.A.; Izadi, M.N.H.; Zaini, M.A.; Radzi, M.; Azis, N. Effect of temperature on a poly-crystalline solar panel in large scale solar plants in Malaysia. In Proceedings of the IEEE Conference on Energy Conversion (CENCON), Johor Bahru, Malaysia, 19–20 October 2015; pp. 244–248. [CrossRef]
4. Sabri, L.; Benzirar, M. Effect of Ambient Conditions on Thermal Properties of Photovoltaic Cells: Crystalline and Amorphous Silicon. *Int. J. Innov. Res. Sci. Eng. Technol.* **2014**, *3*, 17815–17821. [CrossRef]
5. Sahri, A.; Toumi, S.; Ramenah, H.; Tanougast, C. Temperature effects on the power production based photovoltaic cells. In Proceedings of the 25th International Conference on Microelectronics (ICM), Beirut, Lebanon, 15–18 December 2013; pp. 1–4. [CrossRef]
6. Elnozahy, A.; Rahman, A.K.A.; Ali, A.H.H.; Abdel-Salam, M.; Ookawara, S. Performance of a PV module integrated with standalone building in hot arid areas as enhanced by surface cooling and cleaning. *Energy Build.* **2015**, *88*, 100–109. [CrossRef]
7. Elnozahy, A.; Rahman, A.K.A.; Ali, A.H.H.; Abdel-Salam, M.; Ookawara, S. Thermal/Electrical Modeling of a PV Module as Enhanced by Surface Cooling. *J. Clean Energy Technol.* **2015**, *4*, 1–7. [CrossRef]
8. Røyne, A.; Dey, C.; Mills, D. Cooling of photovoltaic cells under concentrated illumination: A critical review. *Sol. Energy Mater. Sol. Cells* **2005**, *86*, 451–483. [CrossRef]
9. Bahaidarah, H.M.S. Experimental performance investigation of uniform and non-uniform cooling techniques for photovoltaic systems. In Proceedings of the IEEE 42nd Photovoltaic Specialist Conference (PVSC), New Orleans, LA, USA, 14–19 June 2015; pp. 1–4. [CrossRef]
10. Cazzaniga, R.; Rosa-Clot, M.; Rosa-Clot, P.; Tina, G.M. Floating tracking cooling concentrating (FTCC) systems. In Proceedings of the 38th IEEE Photovoltaic Specialists Conference, Austin, TX, USA, 3–8 June 2012; pp. 514–519. [CrossRef]
11. Colţ, G. Performance evaluation of a PV panel by rear surface water active cooling. In Proceedings of the International Conference on Applied and Theoretical Electricity (ICATE), Craiova, Romania, 16–17 December 2016; pp. 1–5. [CrossRef]
12. Sreejith, C.S.; Rajesh, P.; Unni, M.R. Experimental study on efficiency enhancement of PV systems with combined effect of cooling and maximum power point tracking. In Proceedings of the International Conference on Inventive Computation Technologies (ICICT), Coimbatore, India, 26–27 August 2016; pp. 1–5. [CrossRef]
13. Adhya, D.; Bhattacharjee, S.; Acharya, S. Back surface cooling of photovoltaic panel—An experimental investigation. In Proceedings of the IEEE 6th International Conference on Power Systems (ICPS), New Delhi, India, 4–5 March 2016; pp. 1–6. [CrossRef]
14. Sun, X.; Dubey, R.; Chattopadhyay, S.; Khan, M.R.; Chavali, R.V.; Silverman, T.J.; Kottantharayil, A.; Vasi, J.; Alam, M.A. A novel approach to thermal design of solar modules: Selective-spectral and radiative cooling. In Proceedings of the IEEE 43rd Photovoltaic Specialists Conference (PVSC), Portland, OR, USA, 5–10 June 2016; pp. 3584–3586. [CrossRef]
15. Raina, G.; Thakur, N.S. Mathematical approach for optimizing heat sink for cooling of solar PV module. *Int. J. Sci. Eng. Res. 2019 (IJSER)* **2019**, *7*, 62–66.
16. Soliman, A.M.; Hassan, H.; Ookawara, S. An experimental study of the performance of the solar cell with heat sink cooling system. *Energy Procedia* **2019**, *162*, 127–135. [CrossRef]
17. Cuce, E.; Bali, T.; Sekucoglu, S.A. Effects of passive cooling on performance of silicon photovoltaic cells. *Int. J. Low-Carbon Technol.* **2011**, *6*, 299–308. [CrossRef]
18. Popovici, C.G.; Hudişteanu, S.-V.; Mateescu, T.D.; Chereches, N.-C. Efficiency Improvement of Photovoltaic Panels by Using Air Cooled Heat Sinks. *Energy Procedia* **2016**, *85*, 425–432. [CrossRef]
19. Hassan, I.A. Enhancement the Performance of PV Panel by Using Fins as Heat Sink. *Eng. Technol. J.* **2018**, *36*, 798–805.

20. Arifin, Z.; Tjahjana, D.P.; Hadi, S.; Rachmanto, R.A.; Setyohandoko, G.; Sutanto, B. Numerical and Experimental Investigation of Air Cooling for Photovoltaic Panels Using Aluminum Heat Sinks. *Int. J. Photoenergy* **2020**, *2020*, 1–9. [CrossRef]
21. Hassan, Y.; Orabi, M.; Ismeil, M.; Alshreef, A.; Al-Rabghi, O.M. Steady State Analysis of Solar Energy Transmitted to Solar Panel in Hot Weather Environment and Various Wind Speed. In Proceedings of the 2019 IEEE International Conference on Sustainable Energy Technologies and Systems (ICSETS), Bhubaneswar, India, 26 February–1 March 2019; pp. 36–44. [CrossRef]
22. Seethamraju, S.; Ramamurthy, P.C.; Madras, G. *Encapsulation for Improving the Efficiencies of Solar Cells*; Materials and Processes for Solar Fuel Production 2014, Nanostructure Science and Technology Book Series; Springer: New York, NY, USA, 2014; Volume 174. [CrossRef]
23. Hammami, M.; Torretti, S.; Grimaccia, F.; Grandi, G. Thermal and Performance Analysis of a Photovoltaic Module with an Integrated Energy Storage System. *Appl. Sci.* **2017**, *7*, 1107. [CrossRef]
24. Hersel, P.; Zweibel, K. *Basic Photovoltaic Principles and Methods*; Solar Energy Research Institute: Golden, CO, USA, 1982.
25. Ramsurn, H.; Gupta, R.B. Nanotechnology in Solar and Biofuels. *ACS Sustain. Chem. Eng.* **2013**, *1*, 779–797. [CrossRef]
26. Dubey, S.; Sarvaiya, J.N.; Seshadri, B. Temperature Dependent Photovoltaic (PV) Efficiency and Its Effect on PV Production in the World—A Review. *Energy Procedia* **2013**, *33*, 311–321. [CrossRef]
27. Anurag, A.; Zhang, J.; Gwamuri, J.; Pearce, J.M. General Design Procedures for Airport-Based Solar Photovoltaic Systems. *Energies* **2017**, *10*, 1194. [CrossRef]
28. Bai, Y.; Chow, T.T.; Ménézo, C.; Dupeyrat, P.; Mé Né Zo, C. Analysis of a Hybrid PV/Thermal Solar-Assisted Heat Pump System for Sports Center Water Heating Application. *Int. J. Photoenergy* **2012**, *2012*, 1–13. [CrossRef]
29. Teo, H.; Lee, P.-S.; Hawlader, M. An active cooling system for photovoltaic modules. *Appl. Energy* **2012**, *90*, 309–315. [CrossRef]
30. Elsafi, A.M.; Gandhidasan, P. Comparative study of double-pass flat and compound parabolic concentrated photovoltaic–thermal systems with and without fins. *Energy Convers. Manag.* **2015**, *98*, 59–68. [CrossRef]
31. Duffie, J.A.; Beckman, W.A. *Solar Engineering of Thermal Processes*, 2nd ed.; John Wiley & Sons: New York, NY, USA, 1991.
32. Cengel, Y.A. *Introduction to Thermodynamics and Heat Transfer*, 2nd ed.; McGraw-Hill: New York, NY, USA, 2008.
33. Alieva, Z.; Nosirov, M.; Mukhtarov, E. The thermal conductivity of solar-cell wafers molded from a powdered stock. *Appl. Sol. Energy* **2014**, *50*, 110–112. [CrossRef]
34. Ngo, I.-L.; Jeon, S.; Byon, C. Thermal conductivity of transparent and flexible polymers containing fillers: A literature review. *Int. J. Heat Mass Transf.* **2016**, *98*, 219–226. [CrossRef]
35. Chen, Y.; Zhuo, F.; Liu, X.; Xiong, L. Thermal modelling and performance assessment of PV modules based on climatic parameters. In Proceedings of the 2015 IEEE Energy Conversion Congress and Exposition (ECCE), Montreal, QC, Canada, 20–24 September 2015; pp. 3282–3286. [CrossRef]
36. Kumar, S.; Mullick, S. Wind heat transfer coefficient in solar collectors in outdoor conditions. *Sol. Energy* **2010**, *84*, 956–963. [CrossRef]
37. Kumar, A.M.; Balasubramanian, M. VAWT which makes use of the turbulent winds generated by the highway traffic. In Proceedings of the IACSIT International Journal of Engineering and Technology, Beijing, China, 16–17 June 2012; Volume 4.
38. Devi, R.; Singh, J. Design and development of prototype highway lighting with road side wind energy harvester. *Int. J. Sci. Res.* **2014**, *3*, 1681–1683.
39. Passmore, M.A. The Measurement and Analysis of Road Vehicle Drag Forces. Ph.D. Thesis, (Aeronautical and Automotive Engineering). Loughborough University, London, UK, 1990. Available online: https://dspace.lboro.ac.uk/2134/7038 (accessed on 1 January 1990).
40. Abdulkareem, S.H.; Al-Obaidi, M.; Sun, L.C. Calculation and optimization of the aerodynamic drag of an open-wheel race car. In Proceedings of the 1st Engineering Undergraduate Research Catalyst Conference, Kuala Lumpur, Malaysia, 1–15 August 2014.

41. Tiwari, G.N.; Sahota, L. Advanced solar-distillation systems basic principles, thermal modeling and its application. In *Green Energy and Technology*; Springer Nature Singapore Pte Ltd.: New Delhi, India, 2017.
42. Migan, G.A. *Study the Operating Temperature of a PV Module*; Project Report; MVK160 Heat and Mass Transfer: Lund, Sweden, 2013.
43. Wenham, S.R.; Green, M.A.; Watt, M.E.; Corkish, R. *Applied Photovoltaics*, 2nd ed.; Earthscan: London, UK, 2006; pp. 33–83.
44. Schwingshackl, C.; Petitta, M.; Wagner, J.E.; Belluardo, G.; Moser, D.; Castelli, M.; Zebisch, M.; Tetzlaff, A. Wind effect on PV module temperature: Analysis of different techniques for an accurate estimation. *Energy Proc.* **2013**, *40*, 77–86. [CrossRef]
45. Skoplaki, E.; Boudouvis, A.G.; Palyvos, J.A. A simple correlation for the operating temperature of photovoltaic modules of arbitrary mounting. *Sol. Energy Mater. Sol. C* **2008**, *92*, 1393–1402. [CrossRef]
46. Ciulla, G.; Brano, V.L.; Moreci, E. Forecasting the cell temperature of PV modules with an adaptive system. *Int. J. Photoenergy* **2013**, *2013*, 192854. [CrossRef]
47. Azzouzi, M.; Popescu, D.; Bouchahdane, M. Modeling of electrical characteristics of photovoltaic cell considering single-diode model. *J. Clean Energy Technol.* **2016**, *4*, 414–420. [CrossRef]
48. Rodrigues, E.M.; Melicio, R.; Mendes, V.M.; Catalao, J.P. Simulation of a solar cell considering single-diode equivalent circuit model. In Proceedings of the International Conference on Renewable Energies and Power Quality, Las Palmas de Gran Canaria, Spain, 13–15 April 2011.
49. Masters, G.M. *Renewable and Efficient Electric Power Systems*; Wiley: Hoboken, NJ, USA, 2004.
50. Sethi, V.P.; Sumathy, K.; Yuvarajan, S.; Pal, D.S. Mathematical model for computing maximum power output of a PV solar module and experimental validation. *J. Fund. Renew. Energy Appl.* **2012**, *2*, 1–5. [CrossRef]
51. Culham, J.R.; Khan, W.; Yovanovich, M.; Muzychka, Y.S. The influence of material properties and spreading resistance in the thermal design of plate fin heat sinks. *J. Electron. Packag.* **2007**, *129*, 76–81. [CrossRef]
52. Cucumo, M.; Ferraro, V.; Kaliakatsos, D. Theoretical and experimental analysis of the performances of a heat sink with vertical orientation in natural convection. *Int. J. Energy Environ. Eng.* **2017**, *8*, 247. [CrossRef]
53. Guitart Corominas, J. *Heat Sink Analytical Modelling*; UPC, Universitat Politècnica de Catalunya BarcelonaTech: Barcelona, Spain, 2011.
54. Song, S.; Lee, S.; Au, V. Closed-Form Equation for Thermal Constriction/Spreading Resistances with Variable Resistance Boundary Conditions. In Proceedings of the IEPS Conference, Atlanta, GA, USA, 11–15 July 1995; pp. 111–121.
55. Werdowatz, A.R. Developing an Empirical Correlation for the Thermal Spreading Resistance of a Heat Sink. Master's Thesis, San Jose State University, San Jose, CA, USA, 2016. Available online: http://scholarworks.sjsu.edu/etd_theses/4711 (accessed on 1 May 2016).
56. Yovanovich, M.M.; Marotta, E.E. *Thermal Spreading and Contact Resistances*; Book Chapter, Heat Transfer Handbook; John Wiley: Hoboken, NJ, USA, 2003.
57. Kraus, A.D.; Bar-Cohen, A. *Design and Analysis of Heat Sinks*; Wiley: New York, NY, USA, 1995.
58. Aweda, J.O.; Adeyemi, M.B. Experimental determination of heat transfer coefficients during squeeze casting of aluminum. *J. Mater. Process Technol.* **2009**, *209*, 1477–1483. [CrossRef]
59. Zell, E.; Gasim, S.; Wilcox, S.; Katamoura, S.; Stoffel, T.; Shibli, H.; Engel-Cox, J.; Al Subie, M. Assessment of solar radiation resources in Saudi Arabia. *Sol. Energy* **2015**, *119*, 422–438. [CrossRef]
60. Almazroui, M.; Tayeb, O.; Mashat, A.S.; Yousef, A.; Al-Turki, Y.A.; Abid, M.A.; Bafail, A.O.; Ehsan, M.A.; Zahed, A.; Rahman, M.A.; et al. Saudi-KAU coupled global climate model: Description and performance. *Earth Syst. Environ.* **2017**. [CrossRef]
61. Rehman, S.; Alam, M.; Meyer, J.; Al-Hadhrami, L. *Long-Term Wind Speed Trends over Saudi Arabia*; King Fahd University of Petroleum and Minerals: Dhahran, Saudi Arabia, 2012. [CrossRef]
62. The General Authority of Meteorology and Environment Protection, Saudi Arabia. Available online: https://www.pme.gov.sa/en/meteorology/pages/climatereport.aspx (accessed on 1 June 2018).